12-18-2000

Growth and Characterization of ZnO for the Front Contact of Cu(In,Ga)Se2

Rita Bhatt
University of South Florida

Growth and Characterization of ZnO for the Front Contact of Cu(In,Ga)Se2 Solar Cells Using Reactive Sputtering Techniques

by

Rita Bhatt

A thesis submitted in partial fulfillment
of the requirements for the degree of
Master of Science in Electrical Engineering
Department of Electrical Engineering
College of Engineering
University of South Florida

Major Professor: Don L. Morel, Ph.D.
Christos Ferekides, Ph.D.
Y.L.Chiou, Ph.D.

Date of Approval:
December 18, 2000

Keywords: ZnO Window Layer, Semiconducting Transparent Thin Films, Al Doped ZnO, Sputtering Parameters, Metal Target Sputtering

ACKNOWLEDGMENTS

I am deeply indebted to my advisor, Dr Don Morel, for his invaluable guidance and patience throughout this study. I would also like to thank Dr. Chris Ferekides for his timely suggestions and Dr Henley for his assistance.

I would like to express my special thanks to all the fellow researchers for their support and friendliness, which has made working in this lab a memorable experience. I thank Raj, Harish and Zafar for the processing assistance.

My special appreciation goes to Sharifa and Binita for their support and invaluable friendship. I deeply thank my father for his loving guidance and my mother for her support. I am grateful to my brother, Rushi for the constant encouragement. Special thanks go to my loving husband, Hiren, for always being there for me. And finally, a lots of hugs and kisses go to my sweet daughters, Aashka and Anya, for reviving my spirit.

TABLE OF CONTENTS

LIST OF TABLES

LIST OF FIGURES

GROWTH AND CHARACTERIZATION OF ZNO FOR THE FRONT CONTACT OF CU(IN,GA)SE2 SOLAR CELLS USING REACTIVE SPUTTERING TECHNIQUES

Rita Bhatt

ABSTRACT

ZnO window layers for $CuIn_xGa_{x-1}Se_2$ solar cells are grown with a DC sputtering technique instead of a conventional RF sputtering technique. Transparent window layers and buffer layers are sputtered from the Zn target in the presence of Oxygen. The window layer is doped with Aluminum in order to achieve high electrical conductivity and thermal stability. The effect of different sputtering parameters on the electrical and optical properties of the films is elaborately studied. Sets of annealing experiments are also performed. Combinations of different deposition parameters are examined to design the optimum fabrication conditions. We are able to deposit 85% transparent, Al doped ZnO films having 002-axis orientation and $4e^{-4}$ ohm-cm resistivity, which is successfully, used on CIGS solar cells. Resistivity of undoped ZnO buffer layers is varied form 10^{-2} ohm-cm to unmeasurable by varying the sputtering parameters. The performance of a reactively sputtered window layer and a buffer layer have matched the performance of the RF sputtered ZnO on $CuIn_xGa_{x-1}Se_2$ solar cells.

There has been considerable effort to eliminate Chemical Bath Deposition of the CdS buffer layer from CIS solar cell fabrication. The performance of an undoped DC

sputtered ZnO layer is examined on Cd free CIGS solar cells. The ZnO buffer layer is directly sputtered on an underlying CIGS material. The performance of Cd free solar cells is highly susceptible to the presence of Oxygen in the sputtering ambient of the buffer layer deposition [6]. As Oxygen is a growth component in reactive sputtering, the growth mechanisms of the DC-sputtered buffer layer are studied to improve the understanding. The performance of all reactively sputtered ZnO devices matched the values reported in the literature and the results for DC sputtered ZnO on Cd-free solar cells were encouraging.

CHAPTER 1 INTRODUCTION

ZnO is a semi-conducting material, which crystallizes in the hexagonal wurtzite lattice. A large direct band gap (3.2 eV) makes this material transparent in the visible and IR region. Pure Zinc Oxide films are transparent and usually highly resistive. Such a coating is widely used as a buffer layer on solar cells. Non-stoichiometric ZnO films have high conductivity but they are not very stable at high temperatures. ZnO is highly conductive and stable when doped with fluorine, aluminum, gallium or indium. Low resistivity and high transparency in the visible region has made this oxide suitable for the front contact of solar cells.

Zinc Oxide based coatings have recently received much attention because they have advantages over the more commonly used indium (ITO) and tin (TO) based oxide films. ZnO is more transparent in the 400- 800 nm range compared to ITO and TO films. Moreover, Indium oxide and tin oxide are usually more expensive than zinc oxide films.

Thin ZnO films can be deposited with MOCVD, spray pyrolysis, evaporation and sputtering. However, sputtering is the most commonly used technique for solar cell applications. The RF magnetron sputtering technique has been widely used for ZnO deposition on Cu (In,Ga)Se_2 solar cells. Atomic beam sputtering and reactive sputtering are also implemented for front contact preparations.

CHAPTER 2 BACKGROUND

2.1 $CuInSe_2$ Solar Cell

The CIS solar cell is a heterojunction P-N diode. The bandgap of CIS is 1.0 eV and measured value of the absorption coefficient is 3-6x10^5 cm^{-1}. The higher absorption coefficient and the low cost processing makes CIS solar cell a leading candidate for thin film solar cells. The highest efficiency that is reported in any compound semiconductor thin film is 17.1 %, which was achieved with a CIGS solar cell [1]. Moreover the CIGS solar cell is stable as well as less toxic compared to other thin film solar cells, *e.g.,* CdTe [2].

2.1.1 Device Structure

Figure 1 shows a schematic diagram of a CIS solar cell. Soda lime glass has been successfully used as a substrate material for solar cells. A back contact of this cell is a thin layer of Molybdenum. Low resistivity in the range of 10^{-5} ohm-cm and the smooth surface of molybdenum result in low series as well as low shunt resistance of the device.

A p-type CIS absorber layer is grown on the Molybdenum surface. CIS has a bandgap of 1.0 eV and an absorption coefficient in the range of 3-6 x 10^5 cm^{-1}. Most of the sunlight is absorbed in less than one-micron thickness of this material.

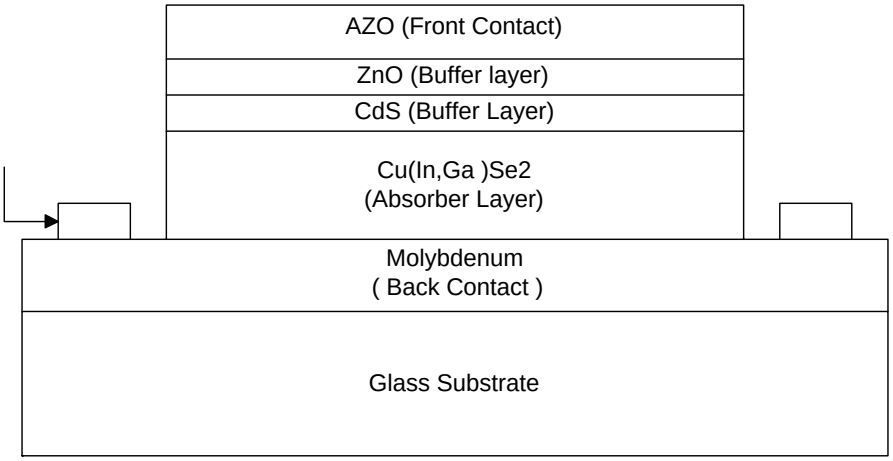

Figure 1 Structure of CIS solar cell

An n-type CdS buffer layer is used between the CIS absorber layer and the ZnO window layer. This layer behaves as an absorber layer for the photons having energy higher than the band gap of CdS i.e. 2.4 eV. On the other hand, for low energy photons, CdS behaves as a window layer material. The CdS layer protects the underlying CIS from oxygen during the window layer deposition [3]. CBD process of the CdS deposition also modifies the underlying CIS surface [4]. Many groups have reported improvement of the open circuit voltage (Voc) and the fill factor (FF) when a thin CdS buffer layer was introduced [6, 7]. CBD CdS has been used for the best $Cu(In,Ga)Se_2$ devices with efficiency above 16% [5].

A resistive layer of ZnO is deposited between a CdS buffer layer and the n-type doped ZnO window layer. Typical resistivity of this layer is 20 ohm-cm. Solar cells without any intrinsic ZnO exhibit the strong decrease in Voc with heating duration. Either the diffusion of Al species from the conductive ZnO:Al or an enhanced diffusion of atmospheric species (O_2 or H_2O) in to the CdS/CIS material could explain the

degradation behavior [8]. A 100–200 nm thick undoped ZnO layer should be deposited to ensure the stability of the device.

Surface resistivity of the front contact of a solar cell must be in the range of 4-10 ohm-cm^2 in order to control the series resistance of a device. A thin layer of Al doped ZnO has been successfully used as a front contact material of the CIS solar cell. The wide band gap (3.2 eV) of ZnO makes it transparent for the IR and visible spectrum of the light.

2.1.2 Operation

A heterojunction solar cell is a p-n diode formed with two dissimilar semiconductors. Figure 2 [9] shows the band diagram of a typical heterojunction solar cell.

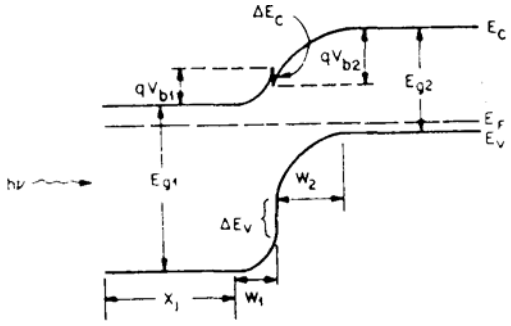

Figure 2 Energy band diagram of an n-on-p heterojunction in thermal equilibrium [9]

The semiconductor material with a higher band gap acts as a window for light in a heterojunction solar cell. This layer is practically transparent to the useful light. Sunlight is absorbed in the second layer of a narrow band gap material. This layer is known as an absorber layer. An electron–hole pair is generated in the absorption layer as a result of the absorption of photon energy. Electrons generated in the p-side within the diffusion length of the junction are swept by the electric field to the n-side. Similarly light generated holes

are drifted from the n type material to the p type material. Light generated current is collected at the output contacts.

I-V characteristic of a solar cell is give by [9]

$I = Is(e^{qv/kt} - 1) - I_L$

Where Is is diode saturation current and I_L is a current resulted by the excitation of the excess carriers due to the solar radiation. This equation is plotted in Figure 3. The curve passing through the fourth quadrant represents negative power. In this mode, power is extracted from the solar cell.

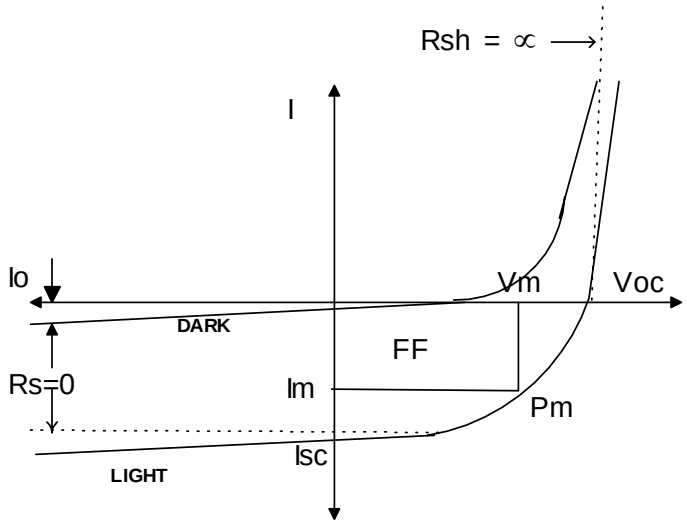

Figure 3 I-V characteristic for solar cell

The performance of a solar cell is interpreted from the photovoltaic efficiency. The efficiency of a solar cell is a measure of light energy successfully converted to electrical energy.

$\eta = Pm/Pin = FF * Isc*Voc / Pin$

Where Voc is open circuit voltage and can be given by

$Voc = A_0 (kT/q)\ \ ln[(Isc/I_0)+ 1]$

Isc is short circuit current and Io is reverse saturation current. Ao is a diode quality factor. The value of Ao can be approximated from the slope of dark I-V data between 0.2V and 0.6V. Io can be calculated from the y intercept of a dark I-V curve. Short circuit current Isc can be obtained from the y intercept of a light I-V curve.

Fill factor FF is given by

$FF = VmIm/VocIsc$

Where Vm and Im are the maximum current and the voltage corresponding to the maximum power point.

A practical solar cell includes the series resistance from ohmic loss in the front contact and the shunt resistance from the leakage currents. An ideal solar cell has negligible series resistance and infinite shunt resistance. Decrease in shunt resistance in a solar cell is mainly due to the defects like pinholes. I-V characteristics of such cells can be given by [9].

$$\ln\left(\frac{I + I_L}{Is} - \frac{V - IRs}{IsRsh} + 1\right) = \frac{q}{kT}(V - IRs)$$

The low shunt resistance decreases FF and Voc of the solar cell whereas the high series resistance decreases FF and Isc of the cell.

2.2 Properties of Semiconducting Transparent Thin Films

2.2.1 Semiconductor Properties

Semiconductor materials, implied by the name itself, have electrical conductivity intermediate between metals and insulators. Conductivity of an intrinsic semiconductor material is due to the atomic arrangement of the material. Silicon, Germanium, GaAs are the examples of such materials. Conductivity of an extrinsic semiconductor material arises due to the presence of impurities, which may be added in the precisely controlled amount. Al doped ZnO is among the extrinsic semiconductor materials.

2.2.2 Electrical Properties

All known semiconductor oxides have n-type conductivity. The following discussion is mainly for the n type semiconductors where electrons are the majority carriers.

According to the Ohms law when electric field E is applied to a material, current density is given by

$J = \rho E$

Where ρ is known as electrical resistivity. Resistivity of the material is related to the mobility and the carrier concentration according to following relation.

$$\rho = \frac{1}{eN\mu}$$

Where N is electron density, μ is mobility of an electron and e is the electron charge. The expression of mobility is

$$\lambda = e\tau / m^*$$

Mobility of free carriers depends upon the relaxation time (Γ), which further depends upon the drift velocity and the mean free path of the charge carriers. These parameters, in turn, depend upon the mechanism by which the carriers are scattered due to the lattice imperfection. A brief account of the various scattering mechanisms involved in semiconductors is given here.

a) Lattice Scattering

In addition to the various stationary imperfections, lattice vibration also distorts perfect lattice periodicity. Lattice vibrations are categorized in to the acoustical and optical modes. This scattering is a strong function of temperature, material density, crystal structure and lattice imperfections. Lattice scattering is a dominant scattering mechanism in the single crystal undoped ZnO.

b) Neutral impurity Scattering

The mobility due to neutral impurity scattering is [10]

$\mu=2\Pi\ m^*e^3/20h\ (N_n)^{-1}$

Where Nn is the concentration of the neutral impurities, m* is the effective mass of an electron and h is Planck's constant. It is clear from above relation that mobility is inversely proportional to the concentration of neutral impurities.

c) Ionized Impurity Scattering

Of all the impurities that may be present in the crystal, the greatest effect on the scattering of the carrier is produced by the ionized impurities. This is because the

electrostatic field due to such impurities remains effective even at a great distance. The corresponding relation for mobility is [11]

$\mu=(4e/h)(\Pi/3)^{1/3}N^{-2/3}$

Where, N is a concentration of the ionized impurities.

Domination of the ionized impurity scattering is reported for the Al doped ZnO films with carrier concentration higher than $4x10^{20}$ cm^{-3} [12].

d) Electron-Electron Scattering

Electron-electron scattering has little influence on mobility because in this process total momentum of the electron gas is not changed.

e) Grain Boundary Scattering

Grain boundary scattering is an important mechanism for the polycrystalline ZnO films. In the polycrystalline thin film, conduction mechanism is dominated by the inherent inter crystalline boundaries (grain boundaries) rather than the inter-crystalline characteristics.

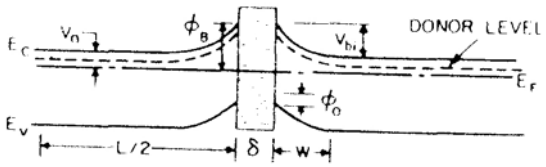

Figure 4 A semiconductor grain boundary interface in thermodynamic equilibrium [13 - fig 3.18]

Grain boundaries generally contain high densities of the interface states. Free carriers from the bulk of the grain can be trapped here, giving rise to the space charge region in

the grain boundary as shown in Figure 4. Band banding occurs due to this space charge region. This band banding introduces potential barriers for the charge transports. In such a situation, mobility of the film (μ_h) is a sum of contributions from bulk (μ_{bulk}) as well as grain boundaries (μ_g).

$$1/\mu_h = 1/\mu_{bulk} + 1/\mu_g$$

In a lightly doped material or at high temperature, thermionic emission over the barrier dominates. Thermionic activated mobility in this case will be given by [14, 17]

$$\mu_g = \mu_0 T^{-1/2} \exp(-e\Phi_b/KT)$$

$$\mu_0 = M/n_c kT$$

Where Φ_b is a height of the potential barrier, n_c is a number of crystallites per unit length along the film and M is a factor that is barrier dependent. Mobility defined in above relation can be approximated as a total mobility of the film as the mobility in the crystallites is much higher than that of the grain boundary.

In the polycrystalline films, when a semiconductor is heavily doped or at low temperature, the dominating current is due to the thermal field emission (tunneling) of the carriers through the barriers. When $E_{00} >> kT$ thermal field emission comes in to the picture. Where [15, 16]

$$E_{00} = 18.5 \text{ X } 10^{-12} (N/m^*\varepsilon)^{1/2}$$

For ZnO films $m^*=0.38$ and $\varepsilon = 8.5$. At the room temperature $N=6x10^{18}$ satisfies $E_{00}=KT$. This indicates that mobility of the sample with carrier concentration higher than this

value will be limited by both thermionic and thermal field emission at the grain boundary [17].

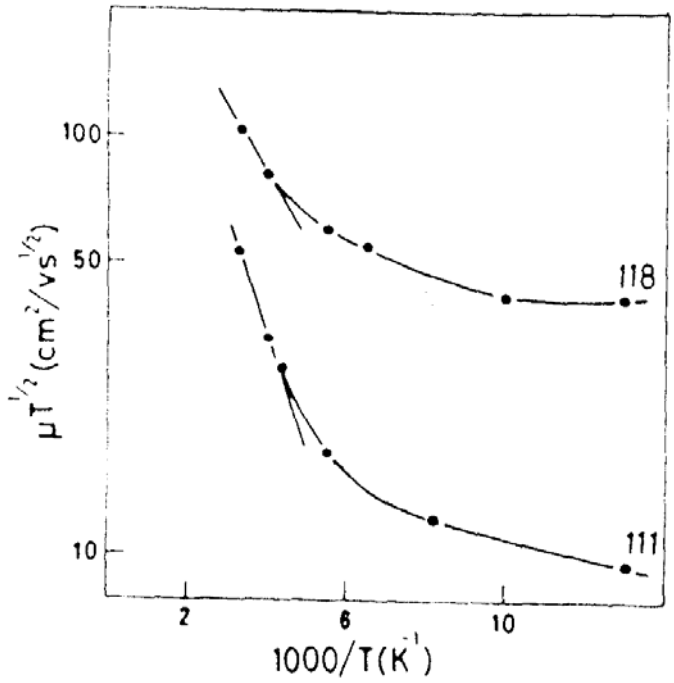

Figure 5 Variation of $\mu_h T^{1/2}$ versus 1/T for CVD grown ZnO films [17 - fig 3.64]

From Figure 5, it is clear that mobility is dominated by tunneling below 100K and conduction is due to both tunneling and thermionic emission above 100K for the ZnO film with $N=2.85x10^{19}$ (sample 118)[18]. Conduction is due to the thermionic emission beyond 200K.

2.2.3 Optical Properties

Absorption and reflection of the incident electromagnetic radiation are the deciding factors of transmittance of a transparent thin film. Transparent semiconducting materials in general, act as a selective transitive layer. They are transparent in the visible and near

infrared range and reflective to the thermal infrared radiation Figure 6 [19]. At very low wavelengths, absorption due to the fundamental band-gap dominates. High reflection due to free electrons (free electron plasma absorption) is observed at very high wavelengths.

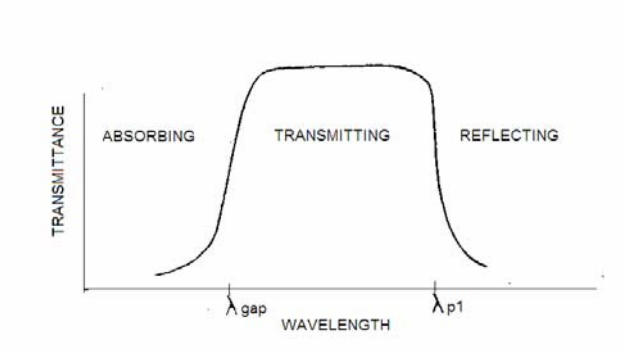

Figure 6 Spectral dependence of a semiconductor transparent material [19 -fig 4.1]

2.2.3.1 Absorption Process in Thin Film Materials

The following absorption processes are responsible for the absorption of electromagnetic radiation in solids. (Figure 7) [13]

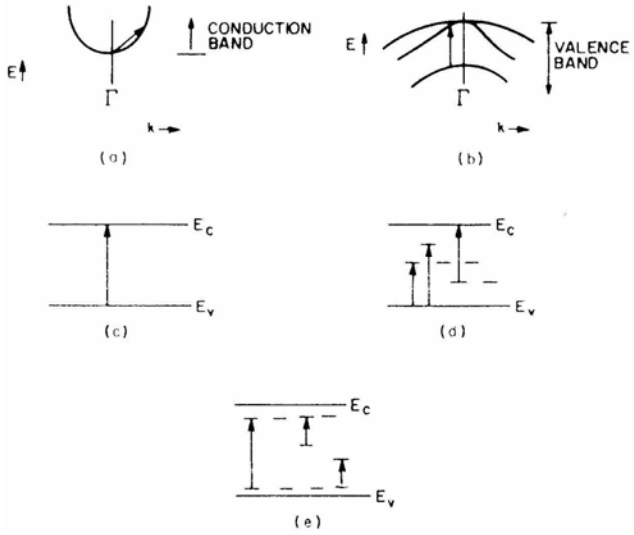

Figure 7 Absorption processes responsible for absorption of electromagnetic radiation in solids [13 -fonash fig 2.12]. a,b-> free carrier absorption. c-> intraband transition. d->band – localize state transition. e->localize state- localize state transition

a) Free Carrier Absorption

This absorption arises from the transition of an electron from the lower energy band to the higher energy band after absorbing a photon within a conduction band. The same kind of transition within the valance band is also possible for a hole. Such transitions are important in the semiconductor whenever the density of the carrier in the band is significant. Absorption caused by the free carrier is characterized by following relation [20, 21]

$$\propto = c\lambda^2 N/\mu$$

Where c is a constant and μ is the mobility of a charge carrier. This relation predicts that absorption caused by the free carriers becomes stronger at longer wavelengths.

b) Phonon Absorption

This absorption normally occurs in the infrared region. Absorbed radiation in this case introduces vibration modes. This kind of process is common in the ionic and covalent materials.

c) Electron Inter-Band Transition.

Electron absorbs photon energy and moves from a single particle stage in the valance band to a single particle state in the conduction band (Figure 7 c). In the direct band gap materials like ZnO, no change in a momentum vector is required for such a transition and phonons are not involved in this absorption process.

Minimum photon energy for a band-to-band transition depends upon the band gap of a material. A valance band electron absorbs the incident photon that has energy higher than the band gap (Eg) of the material. In other words, the fundamental absorption edge occurs for hν=Eg, where ν is a frequency of an incident optical radiation. Variation of the absorption (α) with the photon energy is given by

$$\alpha(h\nu) = C(h\nu - Eg)^{1/2}$$

The absorption phenomenon in a semiconductor with high free electron concentration is explained by Burstein-Moss model [22, 23]. In heavily doped semiconductors, where states near the bottom of the conduction band are filled, transition of an electron is possible only form the valance band to the conduction band states lying above the degeneration Fermi level. This shifts an optical band gap from Eg to the higher energy Egd. This degeneration energy gap is given by

$$E_{gd} = Eg + (h^2/8\Pi^2 m^*)(2\Pi^2 n)^{2/3}$$

The fundamental absorption edge in this case shifts toward the lower value of the wavelength.

In a polycrystalline film, localized states are present in the forbidden energy band gaps. These localized states arise from broken chemical bonds, impurities and other structural defects. This could involve the electron transitions from the localized states and a band (Figure 7 d) and the transitions between the localized bandgap (Figure 7 e). Electrons in the valance band can absorb photon energy less then Eg and transit to the localized state. This may also be true for the transition of an electron from one localized state to the other

localized state. Localized states within the forbidden energy band cause the absorption of a photon with energy less than the band gap energy (Eg) of a material.

2.2.3.2 Correlation of Optical and Electrical Properties

a) Effect of Carrier Concentration on the Optical Band Gap:

According to the Burstein-Moss band-filling model, optical band-gap of a film increases as the carrier concentration increases, as shown in Figure 8 [24]. It is clearly seen from Figure 9 [25] that, as the carrier concentration increases, band edge shifts towards the lower wavelengths.

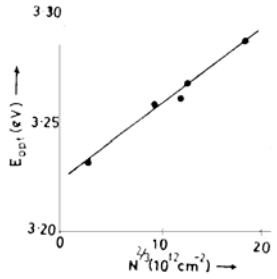

Figure 8 Plot of band-gap (E_{opt}) verses $N^{2/3}$ [24 (fig 4.91)]

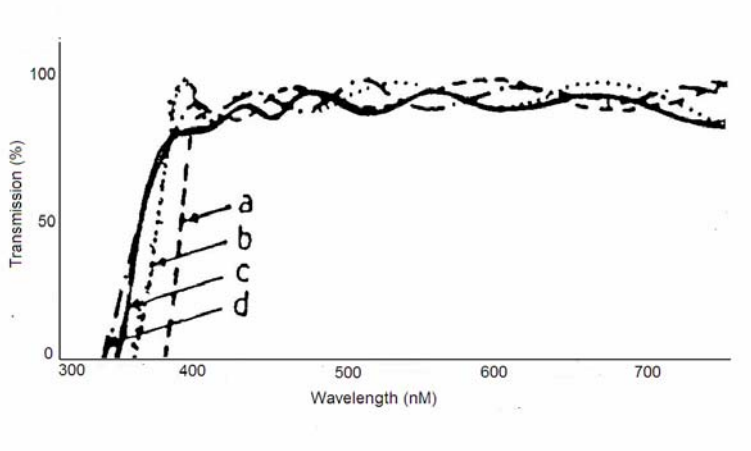

Figure 9 Optical transmission spectra for undoped, 0.5,1.0 and 2wt% Al doped ZnO films [25 fig 4.96]

b) Effect of Carrier Concentration on IR Absorption

Effect of the free carrier absorption is predominantly seen near the infrared wavelengths in the semiconductors such as ZnO. This phenomenon puts an upper limit on the carrier concentration of the transparent conductive oxides.

2.3 Deposition Techniques for Thin Films

Different techniques can be utilized for the deposition of thin films. Deposition processes like spray pyrolysis, sputtering, vacuum evaporation and MOCVD have been successfully used for thin film oxides. ZnO thin films were deposited with reactive sputtering during this study. The following topics briefly describe the sputtering deposition and compare sputtering process with other deposition techniques.

2.3.1 Sputtering Deposition

Sputtering is a process where material is dislodged and ejected from the surface of a solid due to the momentum exchange associated with surface bombardment by the energetic particles. Figure 10 [26] shows the schematic drawing of a sputtering device.

The source of the coating material is called the target and it is placed in a vacuum chamber along with the substrate. The bombardment species are generally ions of a heavy inert gas. Argon is the most commonly used sputtering gas.

Potential is applied between anode (substrate) and cathode (target) to ignite the glow discharge. DC voltage is generally applied between two electrodes when the sputtering target is a good electrical conductor. Non-conducting targets are not sputtered with direct current methods because of the charge accumulation on the target surface. This difficulty

can be overcome with the use of radio frequency (13.56 MHz) sputtering. Deposits of poorly conducting metallic compounds can also be formed by DC sputtering the metallic component while injecting other constituents in the gas phase. This is known as reactive sputtering.

In magnetrons sputtering, a magnetic field is used with the cathode surface to form electron traps. This increases the deposition rate at low substrate heating. Cylindrical-post magnetrons, planner magnetrons and gun type magnetrons are the most commonly used types in the electronics industries.

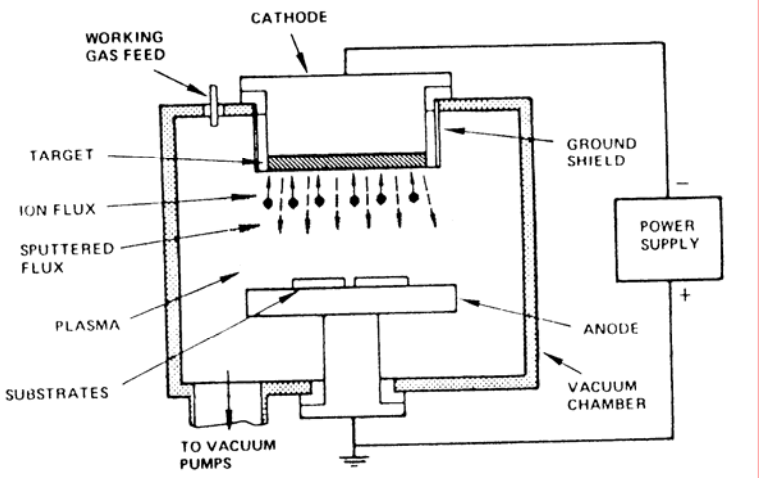

Figure 10 Schematic drawing showing the glow discharge sputtering apparatus of the planar diode type [26 Fig 19]

2.3.2 Comparison of Growth Techniques

Properties of the deposited oxides significantly depend on the growth techniques. Comparison of the characteristics of the ZnO films grown by different deposition techniques is shown in Table 1 [17]. This table enables us to draw following observations related to the sputtering technique.

Disadvantages of Sputtering Technique

a) Low deposition rates

CVD is recommended for the growth of reproducible devices where deposition rate is the primary requirement.

b) Substantial heating of the substrate due to its bombardment by secondary electrons and high-energy ions

Ion assisted growth techniques are preferred over the sputtering for deposition on the polystyrene like materials where substrate heating is not allowable.

c) More complex and expensive process

Spry pyrolysis can be employed for the growth of low cost film where uniformity is not required.

Advantages of Sputtering Technique

a) Higher Purity

b) Better controlled composition

c) Provides films with better adhesive strength

d) Permits better control of the film thickness

e) Versatile

Table 1 Properties of ZnO films grown using different techniques

Process	Substrate Temperature (°c)	Rate (Å/min)	Resistivity (Ohm-cm)	Transmission (%)	Ref.	Remarks
ZnO						
Spray	400	_	10^{-2}	70	17	Annealing in N2
Reactive Evaporation	150-200	_	$1.5x\ 10^{-3}$	89	17	-
Sputtering	200-250	_	10^{-2}	80	17	O_2 = 1-2%
Sputtering	125	_	$2\ x10^{-3}$	90	17	Sputtering in H2
Bias Sputtering	Room	-	$7\ x\ 10^{-3}$	~80	17	5%H2/Ar
ZnO:Al						
CVD	367-444	-	$3\ x10^{-4}$	85	17	-
Spray	500	-	$2\ x10^{-2}$	80	17	-
Spray	300-500	-	10^{-3}	85	17	Annealing in H2
Sputtering Magnetron	<100	3-90	$5\ x\ 10^{-4}$	85(Visible+ IR)	47	RF sputtering of ZnO, DC sputtering for Al
Sputtering Magnetron	350	200	3-6 x 10-4	85(visible)	53	DC Planner – ZnO+Al2O3 Sintered Target
Sputtering Magnetron	350	-	5 x 19 -4	90(visible+I)	12	DC Reactive Sputtering Zn target
Sputtering Magnetron	Room	150	2 x 10 -4	80 (visible)	46	RF Magnetron ZnO +Al2O3 Target

A graphical comparison of the electrical and optical properties of ZnO films as a function of the process is given in Figure 11 [17]. It is quite evident that aluminum doped ZnO, prepared by the sputtering technique has the best properties. Moreover, a vast range of optical and electrical properties is achieved when sputtering technique is employed for the growth of the transparent conducting oxides.

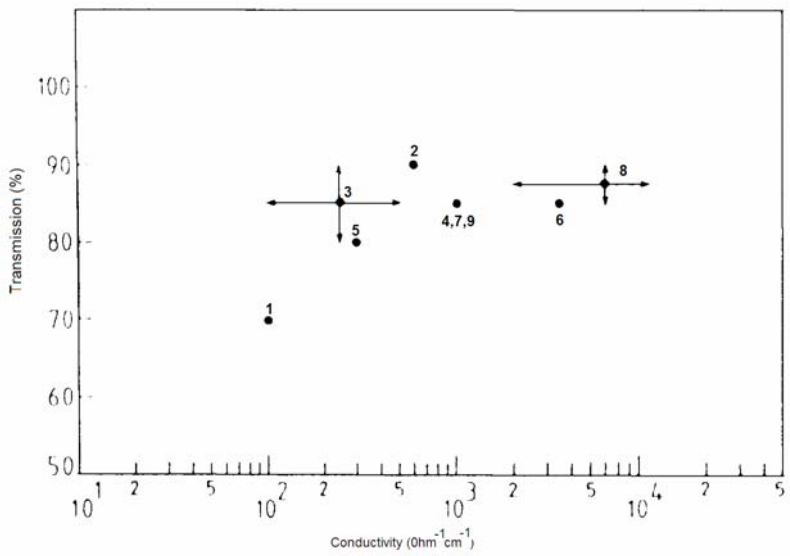

Figure 11 Graphical comparison of electrical and optical properties of doped and undoped ZnO films as a function of growth process [17 fig 2,89]. Undoped: (1) spray, (2) evaporation, (3) sputtering. Doped (4) In-ZnO: spray, (5) In-ZnO: sputtering, (6) Al-ZnO: CVD, (7) Al-ZnO: spray, (8) Al-ZnO: sputtering, (9) Ga-ZnO: sputtering

The sputtering technique, although more complex and expensive, is preferred over any other technique when reproducibility, uniformity and optimum electrical and optical properties of the ZnO film is a prime concern.

CHAPTER 3 MATERIAL PROPERTIES

3.1 Crystal Structure

ZnO crystallizes in the hexagonal wurtzite lattice. The zinc atoms are nearly in the position of hexagonal close packing. Figure 12[27], illustrates the manner in which a zinc crystal model may be constructed. In a ZnO Crystal, every oxygen atom lies within a tetrahedral group of four zinc atoms.

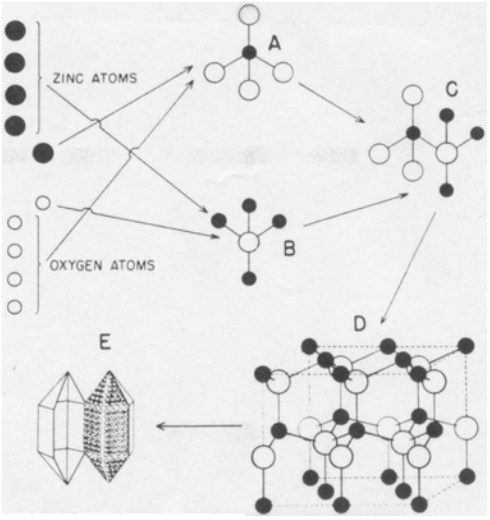

Figure 12 ZnO crystal model [27 fig 1]

The Zn atom gives up two electrons in its outer shell and becomes positively charged Zn++. On the other hand oxygen takes two electrons and become negatively charged O^{--}. This favors the ionic binding. The evidence of the presence of some covalent forces has also been reported in ZnO bonding [27 pg. 15]. The distance between Zn and Oxygen

atoms along ‘c’ axes of the crystal lattice is found to be shorter than the value along the other two axes. This departure of complete tetrahedral symmetry is considered to be due to a covalent bond involving a sharing of electrons by zinc and oxygen atoms along the ‘c’ axis [27].

Table 2 Atomic sizes of Zinc and Oxygen atoms and ions [27]

Zn	1.33 Å	Zn^{++}	0.74 Å
O	0.64 Å	O^{--}	1.40 Å

As shown in the Table 2, O^{--} is a large ion compare to Zn^{++}. As a result, many small atoms can enter a zinc oxide crystal at elevated temperatures.

3.2 Optical Properties

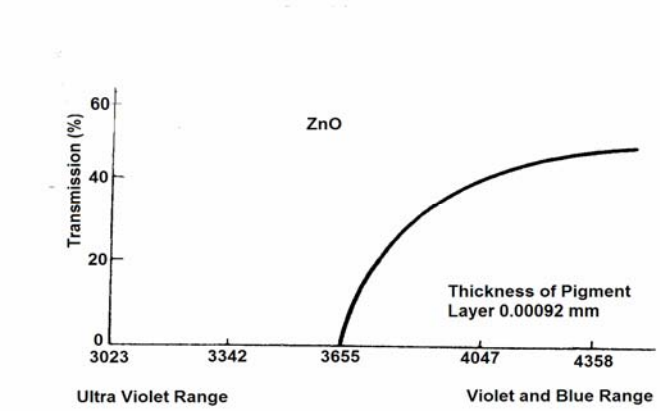

Figure 13 Optical properties of ZnO [27 - ZnO red pg 24 fig 3]

The fundamental band gap of ZnO is 3.2-3.3 eV at room temperature [29]. Optical transmission of ZnO is shown in Figure 13 [27]. ZnO completely absorbs ultraviolet rays

of the spectrum. In other words, ZnO is black in the ultraviolet light. Refractive index of ZnO is 2.2.

3.3 Semiconductor Properties

The semiconductor property of ZnO is mainly due to the imperfection in the ZnO composition. Like all other semiconductor oxides, imperfection in the crystal structure liberates extra electrons and makes this oxide an n-type semiconductor. Following are the possible types of imperfections seen in ZnO composition [27, 17]:

a) Introduction of interstitial atom such as excess Zn

At –220°c, a Zn interstitial atom carries no charge but at room temperature, most of the Zn atoms liberate one electron and becomes positively charged [30, 27].

b) Oxygen vacancies

Oxygen vacancy in the film composition results in the extra electrons liberated from the Zn atom.

c) Substitution of Zn or O by the impurity atoms

d) Impurity atoms at the interstitial sites.

Conductivity of undoped ZnO is mainly due to the imperfections of type a and b [31, 40]. Resistivity of the reactively sputtered undoped film can vary form 10^{2} to 10^{-3} ohm-cm. All undoped films sputtered during this study showed decrement in the carrier concentration when annealed in the inert gas. The decrease in carrier concentration after the heat treatment [chapter 5.3.3] strongly suggested that presence of the interstitial

oxygen, behaving as an acceptor, was negligible in these films. The carrier concentration of the undoped films sputtered during this work was mainly due to the oxygen vacancy or/and interstitial Zn ions. It has also been reported that the undoped conducting ZnO films have unstable electrical properties in a long-term [32].

The imperfections of type c and d can be achieved by doping a film with the trivalent impurities like Al, Ga and In. Resistivity of such films can be as low as 10^{-4} ohm-cm. Dopent content of 0.2 – 0.4 at% is typical for such films. Doping of ZnO not only improves conductivity of the film but also its electrical stability. Electrical properties of the Al doped films are stable up to 650K in vacuum and 450K in Oxygen ambient [33,34]. Table 3 shows some of the important properties of the ZnO film.

Table 3 Properties of ZnO film [17]

Lattice Parameter (A)	a = 3.24, b = 5.20
Dielectric Constant	7.9
Band Gap (eV)	3.2- 3.3
Single Crystal Mobility (cm^2/v-s)	180
Refractive Index	2.2
Electron affinity (eV)	4.2
Melting Point (°c)	1975
Density (gm/cm^3)	5.6

3.4 Application of ZnO

High conductivity, stability and transmission in the visible and IR region make ZnO films suitable for the solar cell applications.

ZnO is extensively used in ceramic industries due to its low coefficient of expansion and high melting point. ZnO has a well-established position in cosmetics and pharmaceutical industries. It provides high covering power, screens out ultraviolet rays, and prolongs effectiveness of perfume [27].

Performance and durability of carbon brushes for a sliding electrical contact are improved by the use of ZnO (~40%). Similarly silver contacts for electrical switching also use ZnO. Up to 66% ZnO is used in electrical and heat insulation. Rubber, paint, adhesive, lubricants, plastics are few more examples of the diversifying use of ZnO in the industry [27].

CHAPTER 4 MATERIAL PROCESSING

4.1 Device Structure

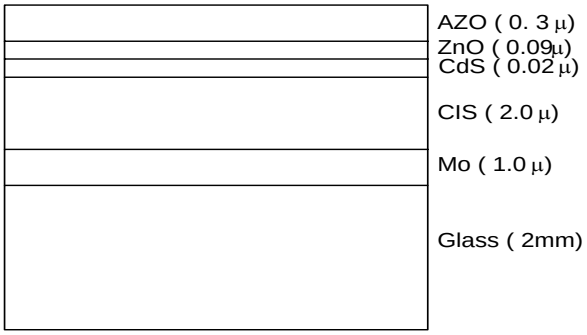

Figure 14 Cross section of CIS solar cell with reactively sputtered window layer

Figure 14 shows the structure of CIS solar cell fabricated under the University Of South Florida solar cell project. The Molybdenum back contact is sputtered on a clean 7059 soda lime glass substrate. The CIGS absorber layer is formed by a two-stage process. In the first stage, the precursor is formed by the sequential deposition of Cu and Ga followed by the co-evaporation of In and Se from the elemental sources. In the second stage, selenization of the precursor is achieved at high temperatures in the presence of Se flux. A thin buffer layer of CdS is deposited by chemical bath deposition process. A thin layer of undoped ZnO is sputtered before the front contact deposition. Al doped ZnO is sputtered to form the window layer of the cell.

4.2 Experimental Setup

ZnO was reactively sputtered using the Veeco 3000 planer magnetron sputtering system. ZnO film was grown on a 4" x 4" soda lime glass substrate. The substrate was mounted on a graphite plate holder and placed 10-15 cm above the target. The substrate was kept slightly off centered in order to avoid the racetrack region of a target. Surface temperature of the substrate was controlled with a heat lamp. A thermocouple was inserted inside the graphite holder to monitor the substrate temperature.

The target material was 3" in diameter and 99.999% pure Zn. Small Aluminum pieces were placed on the target surface to dope a film. A water-cooling system was used to prevent overheating of the metal target.

4.3 Experimental Procedure

Chamber is pumped down to 100 mTorr with a mechanical pump after loading a substrate. The chamber is further evacuated with a diffusion pump. Substrate heating is provided when the pressure drops below 10^{-6} Torr. When the preferred substrate temperature is reached, ultra high purity Argon is flown in to the chamber. DC power is then turned on and the voltage is adjusted. As soon as the glow discharge initiates, the mass flow controller is set for a desired flow of Oxygen and Argon. The flow of Oxygen and Argon is adjusted such that the sputtering pressure is maintained around 3mTorr and the value of sputtering current is maintained within the specified limit. Ratio of the masses of both of the gasses is also kept in the proximity of the selected value.

The shutter is opened when the glow discharge stabilizes. Significant fluctuations of the DC voltage are often noticed during the deposition process. DC voltage is constantly monitored to ensure the stability of the glow discharge. Sputtering voltage is held constant by frequent adjustments of the power source during the film deposition. Occasionally, the flow of the gases has been slightly changed to stabilize the process.

Switch off the DC power and heater when desired thickness of the film is grown. Cut off the gas flow and let the substrate cool down in vacuum. Vent the system when substrate temperature falls below 50°c.

4.4 Processing Parameter for Reactively Sputtered ZnO

4.4.1 Al Doped ZnO

Doping is achieved by placing Al pieces on the target. Table 4 gives the guidelines for the processing parameters suitable for the deposition of AZO.

Table 4 Processing parameters for Al doped ZnO

Base Pressure	1-6 x 10^{-6} Torr
Deposition pressure	2.5 – 4.4 mTorr
Substrate Temperature	100 – 300°c
DC Voltage	480 V
DC Current	140 - 170 mA
% Oxygen	33%
% Argon	67%
Thickness on CIS Solar cell	2500 - 3000Å

4.4.2 Undoped ZnO

Undoped ZnO is sputtered from the Zn target without the Al pieces on it. When Al doped ZnO is sputtered with Al pieces on the target, some portion of the Al liquefies and penetrates into the Zn metal target. The traces of Al are detected in the sputtered film when the same target is used without Al pieces on it. Separate Zn targets are used to sputter doped and undoped layers in order to avoid such cross contamination. Table 5 is a list of recommended processing parameter for ZnO deposition.

Table 5 Processing parameters for undoped ZnO

Base Pressure	1 x 10^{-6} Torr
Deposition pressure	2.5 – 4.0 mTorr
Substrate Temperature	100 – 300°c
DC Voltage	400 - 440 V
DC Current	130 - 155 mA
% Oxygen	38%
% Argon	62%
Thickness on CIS solar cell	900 Å

4.5 Thin Film Characterization Methods

Properties of the film vary significantly according to its position with respect to the sputtered target. As shown in the Figure 15 substrate was divided into five zones according to its position. The region right above the target was labeled ‘Zone A’. The zone away from the target was labeled ‘Zone E’. Damages caused by the high-energy particle bombardment are the least in a region away from the target. Due to this reason,

Zone D and E are used to deposit the window layer on the CIS solar cell. Most of the films discussed in following chapters were deposited in Zone D and E.

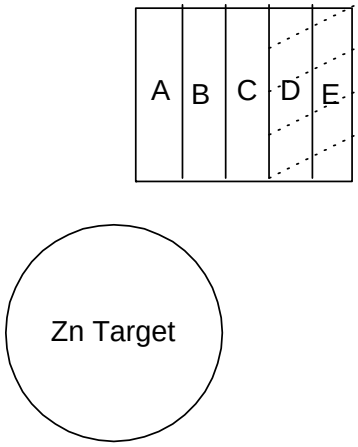

Figure 15 Substrate zones with respect to target

Electrical resistivity of the film was checked by four-point probe method. Following formula was used to calculate sheet resistance and resistivity of the film.

Sheet resistance Rsh = 4.53 (V/I) ohm

Resistivity ρ = Rsh * Thickness of the film in cm

Varian Cary 17 D Photospectrometer was used to measure optical transmission of the film. Absorption coefficient was calculated from the measured value of the transmission with following relation.

Absorption coeff. (cm^{-1}) = ln(measured transmission/10,000) / thickness of the film(cm)

Hall Effect measurement was used to determine carrier concentration and mobility of the majority carriers.

Film composition was determined by standard energy dispersive x-ray spectroscopy (EDS). X-ray diffraction (XRD) was obtained on a Nicolet P3/R3 single crystal diffractometer using Mo radiation with the wavelength of 0.71. Film thickness was measured on Alpha-step 200 profilometer.

CHAPTER 5 RESULTS AND DISCUSSION

5.1 Fundamental Mechanism

5.1.1 Transport Mechanism

The transport mechanism in solids gives rise to the electrical current. The electrical properties of a conductive film are determined by the mechanism by which free electrons transport within the material. Ionized impurity scattering and grain boundary scattering are the most significant scattering mechanisms affecting the mobility of free carriers within the sputtered ZnO film.

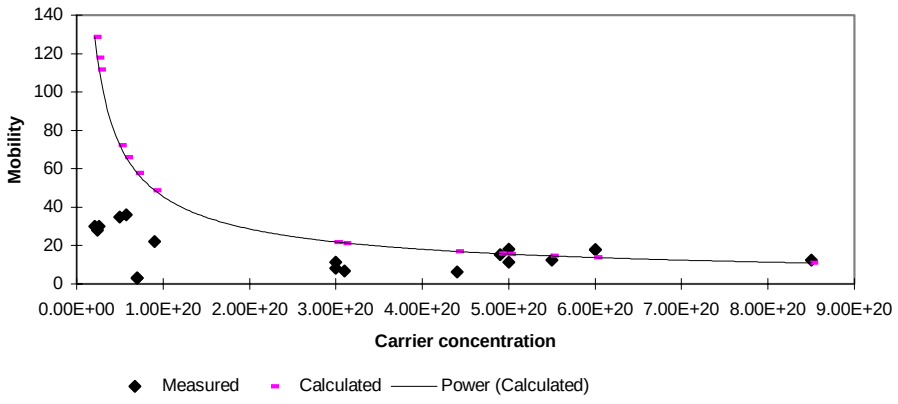

Figure 16 Variation of free carrier mobility with the carrier concentration

Mobility of free electrons is studied to understand the scattering mechanism of the majority carrier within the ZnO film. The mobility affected by ionized impurity scattering is given by the following expression [11].

Free carrier mobility $\mu = (4e/h)(\pi/3)^{1/3} N^{-2/3}$

$$= 9.80 \times 10^{14} N^{-2/3}$$

In Figure 16, the mobility of free carriers is calculated by using the above relation and compared with the measured data. It is clear from the plot that, at higher carrier concentrations, measured data follows the simulated relation for ionized impurity scattering. As depicted in Figure 16, the number of free electrons affected the mobility of the carriers when carrier concentration exceeded $5x10^{20}$ cm^{-3}.

These observations support the reported presumption that the transport mechanism enters into the ionized impurity scattering regime when free carrier concentration exceeds 4 x $10^{20}cm^{-3}$ [12]. The transport mechanism is governed by grain boundary scattering as well as defect induced scattering at the lower carrier concentrations.

Table 6 Electrical properties of undoped ZnO and Al doped ZnO

	ZnO	AZO
Carrier Concentration (n\ cm^2)	8.0×10^{18}	5.10×10^{20}
Mobility	36	18

As shown in Table 6 Al doped ZnO has higher carrier concentration and lower mobility compared to the values for the undoped ZnO films deposited with similar sputtering

settings. Higher concentration in AZO films is attributed to the contribution from Al^{+3} ions on substitutional sites of Zn^{+2} ions and from the interstitial aluminum in the ZnO lattice. Aluminum atoms that produce ionized impurity scattering centers may occupy interstitial positions and deform the structure of the film. Scattering by ionized impurities and defects in the crystal result in the lower mobility seen in doped ZnO films [35, 36, 46].

Table 7 Electrical properties of AZO having different microstructures

Substrate Temperature	Carrier Concentration (cm^{-1})	Mobility ($cm^2/V\text{-}s$)
25ºc	7×10^{19}	3.2
100ºc	5×10^{20}	11
200ºc	6×10^{20}	17.8
325ºc	5×10^{20}	18

Typical carrier concentration of the Al Doped ZnO was 5×10^{20} cm^{-3}. The mobility of these films showed dependence on carrier concentration as well as microstructure of the film. Table 7 shows the electrical properties of films sputtered at different substrate temperatures. The films sputtered at lower substrate temperatures (25ºc – 100ºc) had poor orientation and smaller grain size. The mobility of these films showed more dependence upon the microstructure of the film. This indicated the prevalence of grain boundary scattering and defect-induced scattering. Films that sputtered at higher substrate temperatures had better crystalline structure and showed predominance of ionized impurity scattering.

Typical free carrier concentration of an undoped ZnO film was observed in the range of 5 x 10^{19} cm^{-3}. Full-width at half-maxima (FWHM) of the 002 peaks for the films that sputtered at different temperatures was obtained from XRD measurements and are listed in Table 8. FWHM is a good indication of structural integrity and the grain size of the film. It is clear from this data that mobility improved as crystallinity of the film was improved. From this observation, it can be concluded that the mobility of carriers in undoped ZnO films shows sole dependence on grain boundary scattering and defect-induced scattering. As expected, these films did not show a consistent relation between carrier concentration and mobility.

Table 8 Electrical properties of undoped ZnO having different microstructures

Substrate Temperature (°c)	Carrier Concentration (cm^{-3})	Mobility (cm^2/V-s)	FWHM (Å)
25	9.2 x 10 ^{19}	6.0	-
100	5.7 x 10^{19}	30	0.64
200	5.10 x10^{19}	35	0.54
325	8.0 x10^{18}	36	0.40

5.1.2 Optical Absorption Mechanism

The optical characteristics of polycrystalline ZnO films depend predominantly upon the free carrier concentration, structure, and composition of the film.

5.1.2.1 Effect of Free Carrier Concentration on Optical Absorption

The following are the two main effects of higher carrier concentration on the optical properties of a film:

a) Increase in optical absorption at longer wave lengths

Free carrier absorption is responsible for optical absorption at the longer wavelengths of the spectrum [37]. Films with higher carrier concentrations showed significant increase in absorption at wavelengths longer than 1000 nm (Figure 17). Such reduction in transmission puts an upper limit on the carrier concentration of a conductive transparent film.

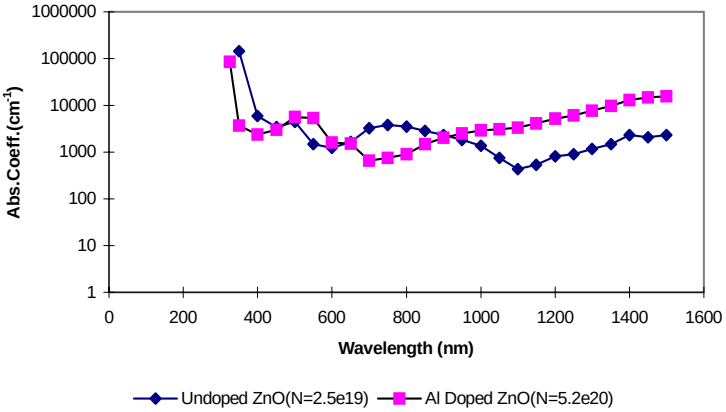

Figure 17 Absorption coefficient v/s wavelength for AZO and ZnO

b) Decrease in optical absorption at shorter wave lengths

Undoped ZnO showed a sharp absorption profile near 350nm, whereas doped ZnO remained transitive at 350nm and became opaque around 325nm (Figure 18). The optical band gaps for both of these films were determined by plotting the square of absorption coefficient's value vs. energy of the incident radiation (Figure 18,). These plots illustrate that the optical band gap of the undoped ZnO film shifted from 3.3 eV to 3.52 eV when doped with Al (Figure 19,). The wider bandgap seen in the doped film

suggests a Burstein-Moss shift [37]. The opening of the band gap explains the decrease in optical absorption at shorter wavelengths.

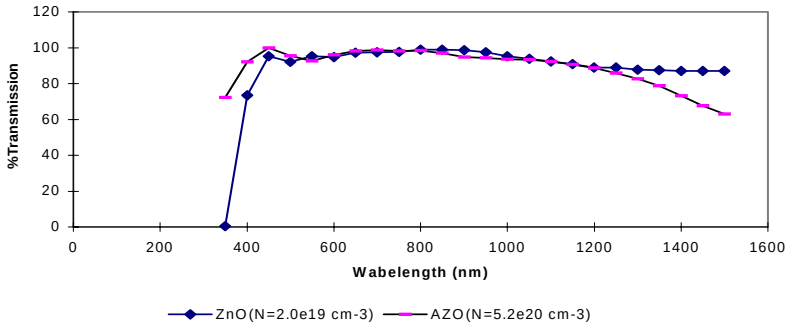

Figure 18 %Transmission vs. wavelength for AZO and ZnO

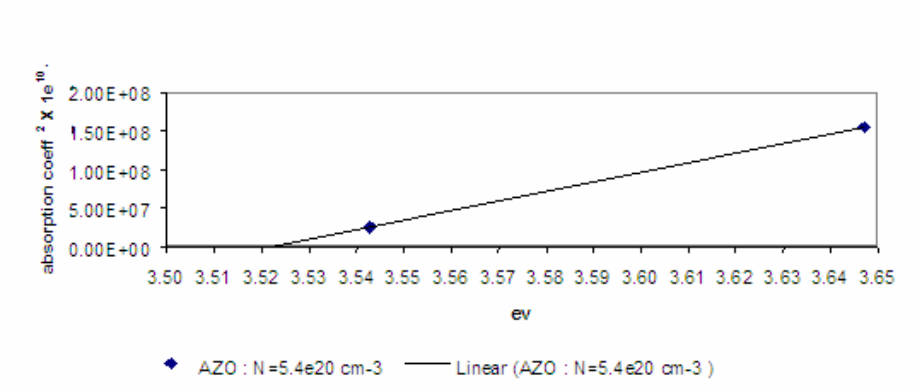

Figure 19 Calculation of optical band gap for Al doped ZnO (N = 5.4e20 cm^{-3})

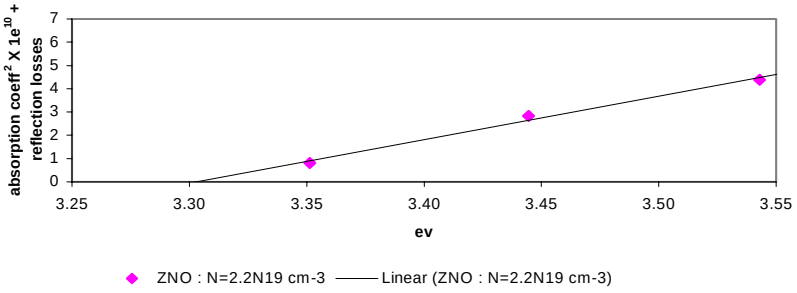

Figure 20 Calculation of optical band gap for undoped ZNO (N = 2.2e19 cm^{-3})

5.1.2.2 Effect of Microstructure on Optical Absorption of ZnO Thin Film

Stoichiometry of the film had considerable effects on the optical properties of the ZnO thin film. ZnO films with different integrity were grown by varying the substrate temperature. Figure 21 compares the optical behavior of undoped ZnO films with various microstructures. XRD analysis of these films is shown in Figure 22,Figure 23 and Figure 24.

We analyzed free carrier concentration and mobility along with the XRD data to see the overall picture of the microstructure of these films. Oxygen vacancies and interstitial Zn generate free carriers in undoped ZnO films [31] which, when deposited at lower substrate temperatures, showed a high higher carrier concentration, which suggested the presence of excess Zn in the composition of the film (Table 8). Thus, lower free carrier concentration in undoped ZnO films indicates better Stoichiometry of the thin layer. The improvement of half width full maxima of the 002 peak seen in less conductive undoped films affirms the enhanced integrity of the material (Figure 22,Figure 23 and Figure 24). Figure 21 distinctly shows that films with better Stoichiometry were more transparent than the inferior films sputtered at room temperature.

Less transmittance of the inferior films can be attributed to the localized states arising from broken chemical bonds, defects, and impurities [38]. Electrons residing in localized states absorb the incident photon energy and transit it to the conduction band. Electron transitions between two localized states and a localized state and the valance band are also feasible [13]. Such transitions were responsible for more absorption of the incident

light. Furthermore, poor microstructure increased scattering of the incident light. Such scattering also contributed to the reduction of transmittance of the film.

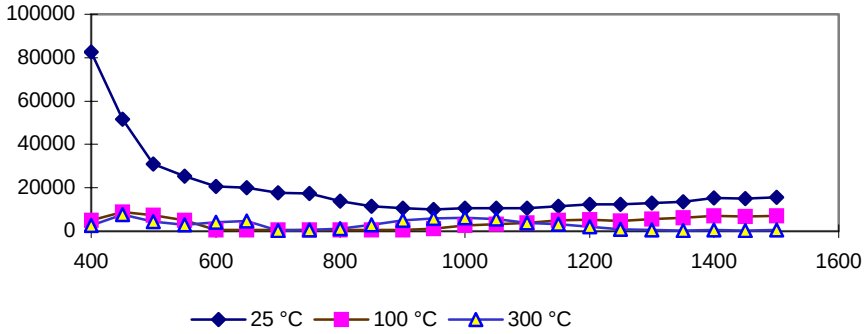

Figure 21 Variation of absorption coefficient as a function of optical wavelength for ZnO films sputtered at different substrate temperatures

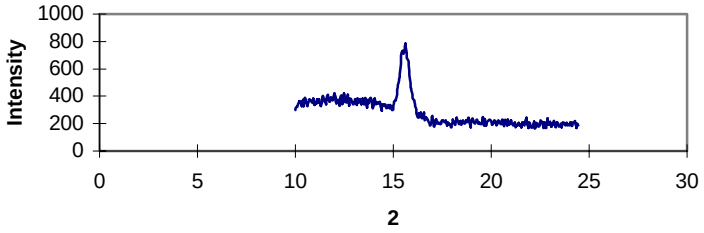

Figure 22 XRD of ZnO deposited at 300°c

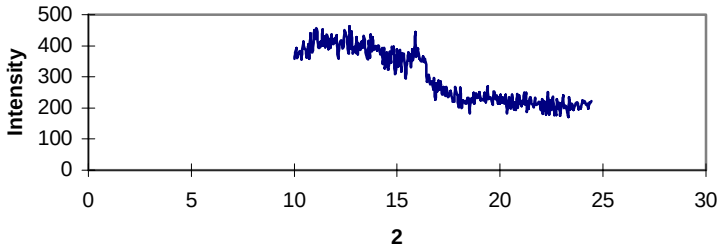

Figure 23 XRD of ZnO deposited at 100°c

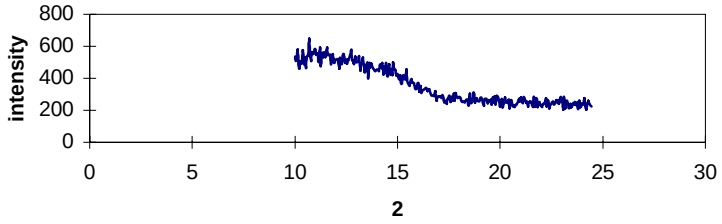

Figure 24 XRD of ZnO deposited at room temperature

It is interesting to note that the effect of stoichiometry on the optical transmission is prominent in the visible range of the spectrum. Shifting of the absorption band into the visible region has been reported with the introduction of excess Zinc into ZnO. This effect has been attributed to the strain caused by excess Zn atoms in the interstitial positions [38]. In order to understand this effect, we studied possible donor levels of the Zn ion in ZnO films. A model of non-stoichiometric ZnO, shown in Figure 25 [27], was used to explain the above observations.

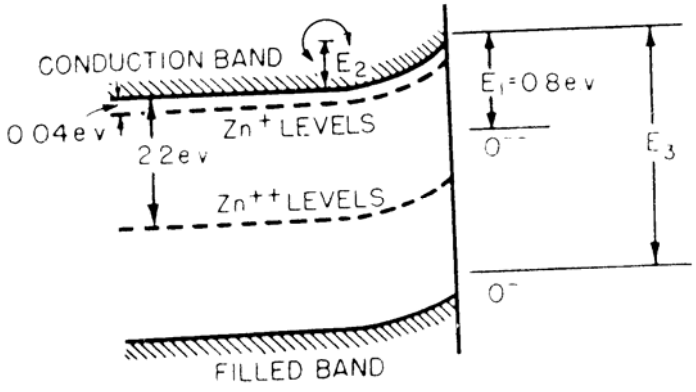

Figure 25 Model of Zinc Oxide [27 pg.58 fig 10]

Table 9 Possible defect levels in undoped ZnO films

Donor/Acceptor Levels	Min Energy Required for Electron Transition from VB to Defect Levels		Min Energy Required for Electron Transition from Defect Levels to CB	
	eV	nm	eV	nm
Zn +	3.26	380	.04	*3100*
Zn++	1.1	1127	2.2	563

Table 9 summarizes the possible defect levels in ZnO and the fundamental absorption edge associated with these levels. Donor levels produced either because of oxygen vacancies or incorporation of hydrogen, indium, lithium, or Zn are reported in the range of 0.02-0.05 eV below the conduction band [17]. In undoped ZnO film, an acceptor level has been reported at 0.80 eV below the conduction band [27]. Wavelengths associated with these energy levels fall in the visible region (380nm – 563 nm) and higher IR region (1550-3100 nm) of the spectrum (Table 9). As shown in Figure 21,the optical behavior of ZnO at frequencies higher than 1500nm was not observed during this study. Influence of microstructure on the transmission of visible light can be partly attributed to the presence of defect levels.

This hypothesis may prove useful to explain the predominant effect of stoichiometry on optical absorption of the visible radiation. Because of the limited nature of the collected data, this presumption requires further research for the justification.

5.2 Effect of Sputtering Parameters on the Growth of a Sputtered ZnO Film

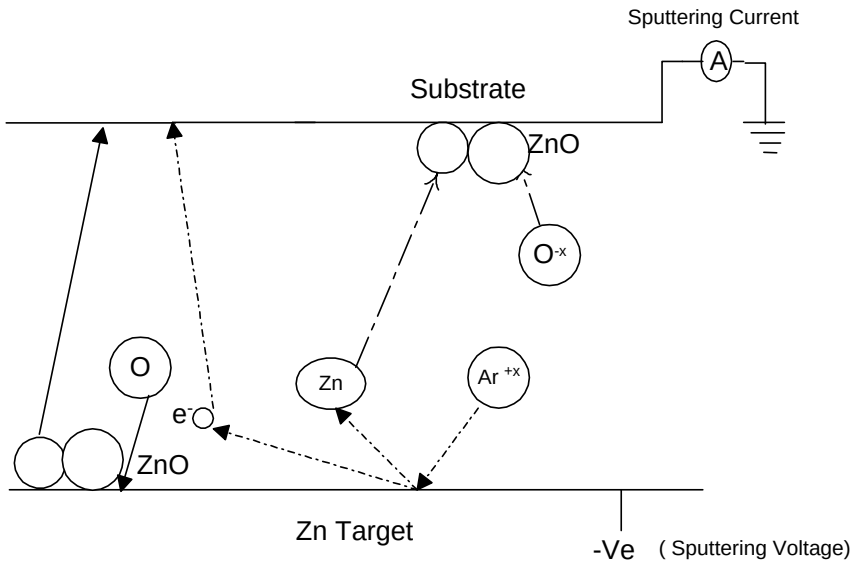

Figure 26 Growth mechanism of reactively sputtered ZnO

The growth mechanism of reactively sputtered ZnO is depicted in Figure 26. Compounds are synthesized at the target or at the substrate in reactive sputtering. Reaction in the gas phase for the most part can be ruled out, as ions cannot be neutralized in the gas phase. The heat liberated in a chemical reaction cannot be dissipated in a two-body collision. Simultaneous conversion of energy and momentum requires the reaction to occur at a surface- either at the target or the substrate [52,26]

At low O_2 injection rate, virtually all of the O_2 is getter pumped by the condensing Zn coating. Consequently the O_2 partial pressure remains relatively low, and the cathode process remains primarily one of the simple Ar sputtering of Zn. Most of the ZnO is synthesized on the substrate. The coatings deposited under these conditions are metallic in nature. In this mode, deposition rate linearly increases with the Oxygen injection rate. As the O_2 injection rate approaches that required to produce a stochiometric ZnO, the O_2

partial pressure rises because of the reduced getter pumping rate [26]. In this mode, formation of ZnO on the target accelerates. As a consequence, the target cathode develops a surface oxide and deposition rate reduces. It is possible that ZnO decomposes when sputtered. Such poisoned targets can produce Zn atoms, Oxygen atoms, ZnO compounds as well as secondary electrons [26]. The same effect can be seen when the sputtering rate of Zn atoms is decreased while the oxygen injection rate is kept constant.

As shown in Figure 27, the deposition rate of sputtered films is governed by the following factors:

a) Sputtering rate of metallic target

Affecting Parameters: Sputtering voltage, gas pressure and O_2 concentration

b) Fraction of the sputtered atom (Zn) that can reach the substrate

Affecting Parameters: Gas pressure, O_2 concentration

c) Fraction of the sputtered atoms that are oxidized ($Zn_{1+x}O$) before they reach the substrate.

Affecting Parameters: Gas pressure, O_2 concentration, sputtering voltage

d) Oxidation rate of sputtered atom on the substrate

Affecting Parameters: O_2 concentration, substrate temperature

5.2.1 Effect of Sputtering Voltage

The following results were taken at different sputtering voltages while keeping other parameters constant. Sputtering current was restrained in the range of 150mA to 200mA. In this case, sputtering power can be considered directly proportional to the sputtering voltage.

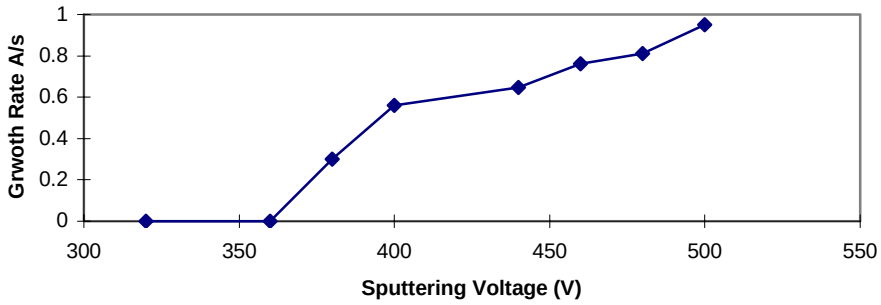

Figure 27 Variation of growth rate of sputtered film as a function of sputtering voltage

As shown in Figure 27, sputtering yield of Zn was achieved between 360 Volts and 380 Volts at 3 mTorr of ambient pressure. The sputtering rate of Zn increased with the sputtering voltage. This resulted in increased deposition rate. Change in the slope of the linear plot at 400 Volts indicates slower growth at voltages higher than 400 Volts. Limited supply of O_2 was responsible for the slower growth at higher voltages.

5.2.2 Effect of Sputtering Pressure

The effect of sputtering pressure was studied by increasing the flow rates of both, O_2 and Ar, without altering their relative concentrations. Data shown in Figure 28 has been taken at constant O_2 to Ar ratio (0.85).

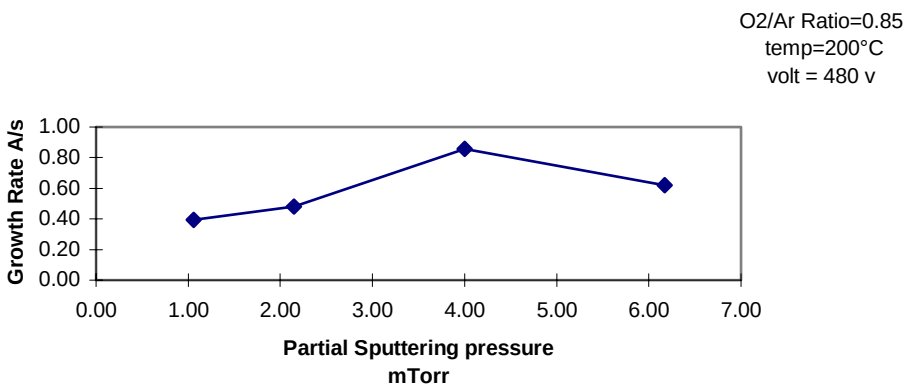

Figure 28 Variation of growth rate as a function of partial sputtering pressure

As shown in Figure 28 a monotonic increase in deposition rate was observed when pressure was raised from 1 mTorr to 4 mTorr. The faster growth of a film can be attributed to the enhancement of O_2 and Ar fluxes.

The higher concentration of Ar flux increased the sputtering rate of Zn atoms from the target. The rise in sputtering current confirmed more sputtering activities at higher ambient pressures (Figure 29). The oxidation rate of sputtered Zn atoms/Ions was also increased at higher sputtering pressures due to the enhancement of O_2 flux. As a result, the deposition rate increased by a factor of two when pressure was increased by 3 mTorr (Figure 28).

The mean free path of a sputtered atom (Zn) decreases at higher pressures. This results in back scattering of the sputtered atom [40]. Enhanced sputtering current could not contribute to the faster growth of the film due to the back scattering. As a result, deposition slowed down above 4.0 mTorr (Figure 29). At higher pressures, unoxidized Zn atoms were scattered all over the sputtering chamber in the form of fine powder.

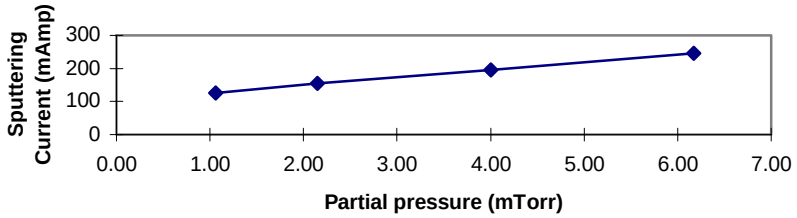

Figure 29 Sputtering current as a function of sputtering pressure

The minimum sputtering pressure, which could sustain the glow discharge was found in the range of 1 mTorr. Below this pressure, secondary electrons could not undergo a sufficient number of ionizing collisions before they struck the anode [26].

The fluctuation of sputtering pressure increased at higher pressures due to the enhanced O_2 flux. The glow discharge became unstable for partial pressure more than 10mTorr. Instability of the discharge in the oxygen rich ambient was also observed when oxygen concentration was increased beyond a certain limit (50%), even at lower sputtering pressures (4 mTorr). Other groups have also reported an influence of oxygen concentration on the stability of the glow discharge. [41,40].

5.2.3 Effect of O_2 Concentration

Oxygen flow rate had been the most important sputtering parameter due to reactive nature of the sputtering. Experiments were carried out with constant sputtering voltage and pressure to study the effect of O_2 concentration on the growth of ZnO Films. Various concentrations of O_2 were achieved by altering the O_2 to Ar ratio at constant pressure. In order to maintain the pressure, the flow of Ar was decreased when the flow of oxygen was increased.

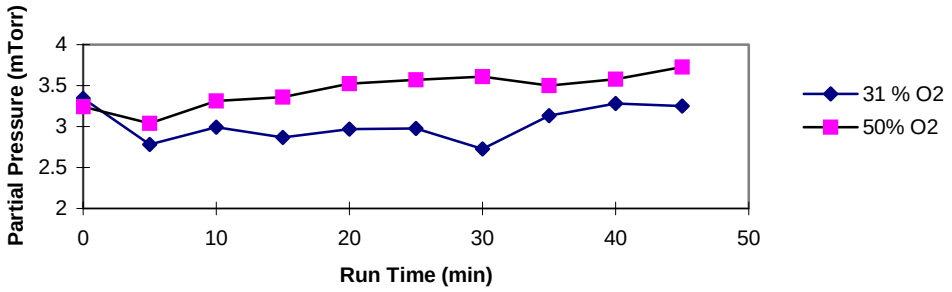

Figure 30 Partial pressure vs. run time for 31% and 50% Oxygen concentrated ambient

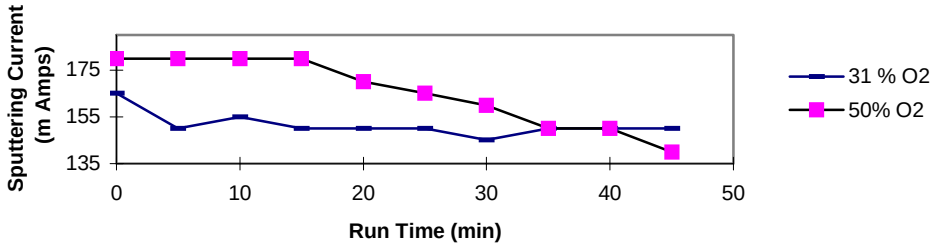

Figure 31 Sputtering current vs. run time for 31% and 50% Oxygen concentrated ambient

When ZnO is reactively sputtered from a Zn target in the presence of Oxygen, there are two competing oxidation processes occurring during the deposition process [41]. One is the oxidation of a deposited film on the substrate, while the other is the oxidation of the Zn metal cathode. Higher Oxygen flow causes rapid oxidation of the Zn target, forming a thin oxide layer on the target. A fraction of the DC applied voltage drops across this layer resulting in lower cathode voltage available to sustain the discharge [26]. Moreover, the sputtering yield of ZnO is lower than that of Zn because the oxide has a higher binding energy and mass than the metal atom [26]. As a result, the increasing depth of the oxidized layer slows down sputtering activities. The deposition rate decreases. This effect is clearly seen in Figure 30 and Figure 31. Sputtering current gradually dropped

from 180mA to 140mA in 45 minutes when the process was stared with 50% Oxygen concentration. Partial pressure increased by 0.69 mTorr during this period. On the other hand, the process carried out with 30% Oxygen concentration maintained practically constant current with 0.47 mTorr increment in the partial pressure. In order to avoid excessive oxidation of the Zn target, an upper limit of the Oxygen concentration was set to 40% during this work.

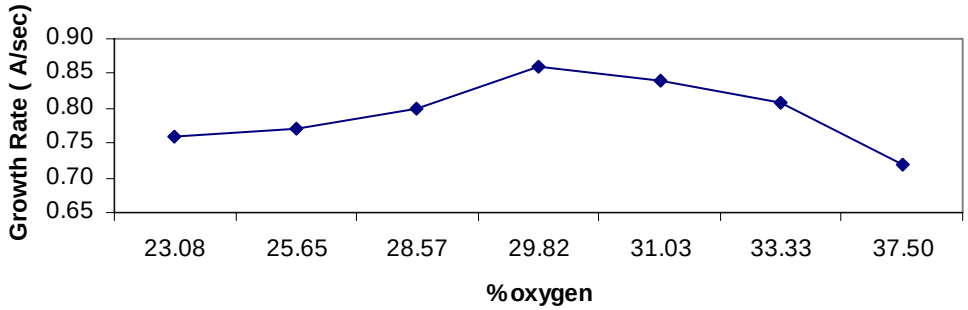

Figure 32 Growth rate as a function of %Oxygen concentration of the films sputtered at 200°c of substrate temperature and at 3 mTorr pressure

Figure 32 shows the dependence of growth rate on oxygen concentration for the films sputtered at 200°c. Acceleration in the deposition rate was observed when oxygen concentration was increased from 22% to 29%. The sputtering rate of Zn could be considered constant for this range of oxygen concentrations, as the sputtering power and pressure were unaltered during this set of experiments. Thus, the increase in deposition rate was the consequences of faster oxidation of the sputtered Zn atoms [42,43,44].

O_2 concentration higher than 29% slowed downs the deposition rate. This is attributed to oxidation of the target itself. Since the binding energy of ZnO is greater than Zn, the reduction in sputtering rate was observed at higher gas phase concentrations. This is

further confirmed by the reported fact that the growth rates obtained using a Zinc target at higher O_2 concentrations were more comparable to the values for a ZnO target [45].

Initial acceleration in growth rate with increasing oxygen concentration and drastic decrement of deposition rate in highly oxygen concentrated ambient is the characteristic of reactive sputtering. Several groups have also reported such behavior. [42,43,44].

Films become oxygen deficient when Oxygen flow is limited. This introduces the lower limit of O_2 concentrations, which was 28.5% (at 3mTorr pressure) with our experimental set up.

5.2.4 Effect of Substrate Temperature

Deposition governed by reaction on the substrate surface depends upon the arrival rate of the sputtered Zn and oxidation rate of this atom ON the substrate surface.

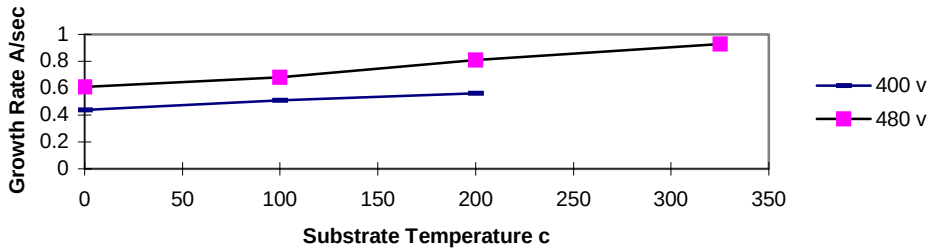

.Figure 33 Growth rate as a function of substrate temperature for the films sputtered with sputtering voltage of 400 Volt and 480 Volt with 30% Oxygen concentration at 3 mTorr sputtering pressure

The relation between substrate temperature activated growth and arrival rate of sputtered Zn was studied with the different combinations of substrate temperature and sputtering voltage. As shown in Figure 33, film growth was more temperature dependent when

films were sputtered at higher voltages. Whereas, when the arrival rate of Zn to the substrate was slower at lower voltages, deposition was less temperature dependent. This suggested that oxidation rate of arriving Zn atoms was sufficient enough to oxidize all the approaching Zn atoms on the substrate surface when the sputtering rate of Zn was slow. Moreover, the rate of ZnO formation ON the target increased when the sputtering rate was decreased [52, pg.42]. Growth of the film was more temperature dependent when the flux of sputtered Zn approached the substrate surface rapidly. At high target sputtering rates, it is well established that virtually all of the compound synthesis occurs at the substrate [52]. At low substrate temperatures and high sputtering voltages, the reaction rate was not fast enough to oxidize all the arriving metal atoms. Accelerated oxidation rate of metallic Zn at higher substrate temperatures resulted in a faster film growth.

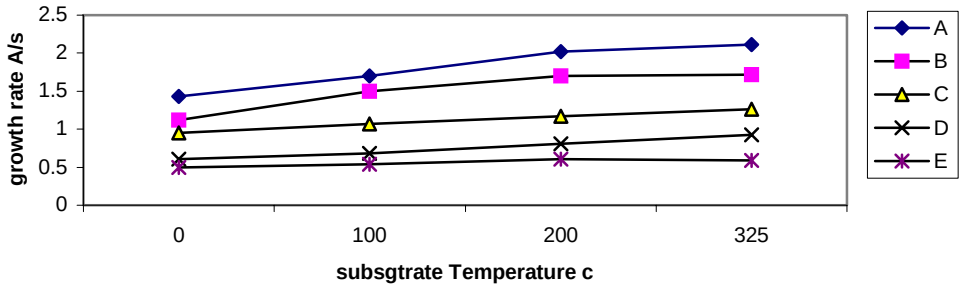

Figure 34 Special distribution of growth rate with different temperatures

This kind of effect was also observed for different substrate positions (Figure 34). The arrival rate of Zn was slow at the region away from the target (region E) whereas Zn atoms rapidly approached the region right above the racetrack (region A). It is clear from Figure 34 that growth is more temperature dependent in region A compared to that of

region E. The effect of high-energy particle bombardment might also have contributed to this result.

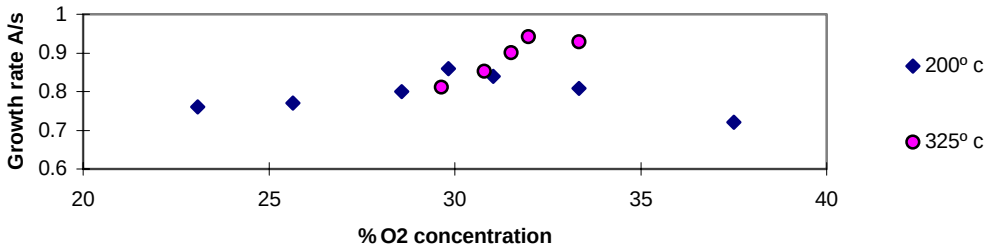

Figure 35 Growth rate as a function of Oxygen concentration for the films sputtered at 200°c and 325°c at the sputtering voltage of 480 V and 3 mTorr partial pressure

Oxygen flux approaching the growing film is another significant factor, which plays an important role in determining the temperature activated reaction regime. As shown in Figure 35, the substrate temperature did not affect deposition rate when the film was sputtered in oxygen concentrations lower than 30%. This was the 'Oxygen starved' regime and oxygen flux was not sufficient enough to oxidize all the arriving metal atoms [28]. In the Oxygen starved regime, a higher rate of reaction did not result in faster film growth. The drop in the growth rate at higher O_2 concentrations can be attributed to the oxidation of the target.

From the above observations, it is safe to conclude that growth was more temperature dependent when sufficient flux of Zn and Oxygen was available near the substrate.

5.3 Effect of Sputtering Parameters on the Properties of the Film

The primary purpose of this work was to develop an optimum sputtering technique for the window layer ZnO. In order to get the best combinations of electrical and optical properties of the film, the effect of different sputtering parameters on deposited films was elaborately studied.

5.3.1 Sputtering Voltage

The DC voltage applied between a Zn target and a substrate is known as sputtering voltage.

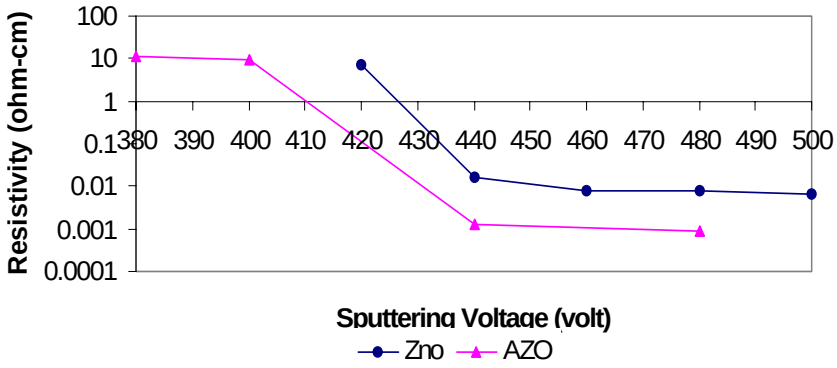

Figure 36 Resistivity vs. sputtering voltage of an undoped ZnO and Al doped ZnO

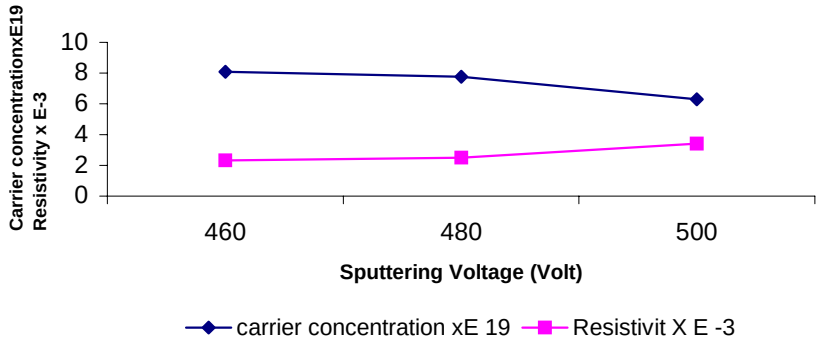

Figure 37 Carrier concentration and resistivity vs. sputtering voltage of the undoped ZnO film

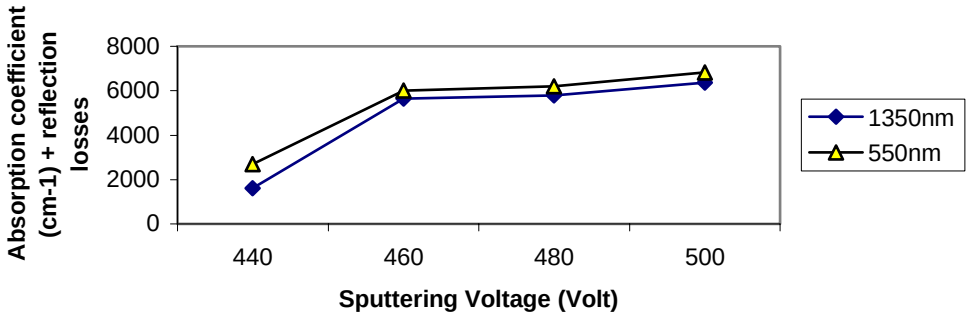

Figure 38 Variation of absorption coefficient of an undoped ZnO as a function of sputtering voltage at 1350 nm and 550 nm wavelengths

As shown in Figure 37, carrier concentration of the undoped film increased with sputtering voltage, which resulted in less resistive films. Transmission of the ZnO also decreased when sputtered with higher voltages (Figure 38). This suggested that film sputtered at higher sputtering voltages were Zn rich, i.e. oxygen deficient. This observation confirmed that conductivity of the undoped films is due to the non-stochiometry in the form of interstitial Zn atom and/or deficient oxygen sites.

It is interesting to note that Al doped ZnO showed threshold effects similar to the undoped ZnO films in above plot. The transition from high resistivity to high conductivity was achieved around 410 Volts for AZO (Figure 36). Undoped films showed such transitions at 425 Volt. This suggested the possibility of oxidation of Al at lower voltages. At lower voltages, the sputtering rate of Al was slow. The relatively higher concentration of Oxygen could be sufficient to partially oxidize Al atoms/ ions. Oxides of Aluminum do not behave as a dopent and do not contribute much to the conductivity of the film (Figure 36). Similar effect was seen when AZO was sputtered with higher oxygen concentrations with 480 sputtering voltage.

As shown in Table 10, Al is a low yield material compared to Zn. The presence of Al in the sputtered film was noticed around 60W with our experimental set up. Deposition of ZnO was initiated approximately at 54W sputtering power. Due to the significant difference between sputtering yields of these two materials, films sputtered at the low voltages had negligible Al incorporation. EDS analysis had indicated a small amount of Al (0 % - 0.3% wt) in films sputtered at lower voltages. At higher voltages, the sputtering rate of Al increased along with Zinc. This resulted in more dopant incorporation inside the growing film. Higher conductivity of the film, seen at higher sputtering voltages, can be attributed to the increased dopant concentration [47 fig 4].

Table 10 Sputtering yield under Argon bombardment [26]

Target	Ion Energy (eV)	Yield (Atom/Ion)
Al	600	1.5
Zn	600	5.07

5.3.2 Sputtering Pressure

The effect of sputtering pressure on the resistivity of the film was not significant (Figure 39) .The increase in resistivity of Al doped ZnO at high pressures may be attributed to the increased oxidization rate of sputtered Al atoms. Moreover, at high pressures the mobility of the free carriers might have degraded due to the higher Al concentration within the film.

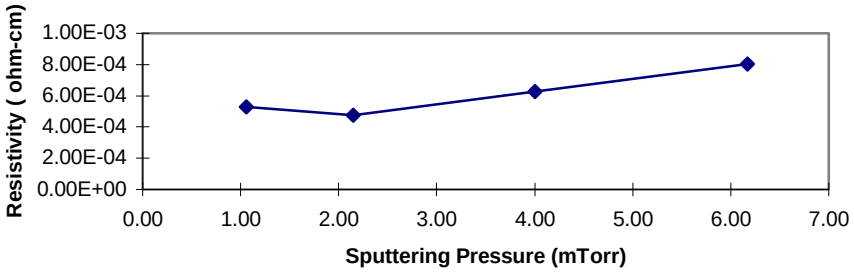

Figure 39 Resistivity of AZO as a function of sputtering pressure

High electrical resistance of the film, sputtered below 2 mTorr, could be attributed to the enhancement of the bombardment by high-energy oxygen, resulting from the increase in the mean free path of these species [48].

5.3.3 Oxygen Concentration

Figure 40 and Figure 41 shows the electrical properties of the undoped ZnO films as a function of oxygen content of the sputtering ambient. When Oxygen concentration was increased from 22% to 33%, free carrier concentration declined from 6 x 10^{19} cm^{-3} to 2.5 x 10^{19} cm^{-3}. Mobility of the free carriers appeared to be unaffected in this range of the concentration.

The reduction in free carrier concentration suggested fewer Oxygen deficient sites within the undoped film. Improved optical transmission, both in IR and visible region of the spectrum, also implied less metal rich stochiometry of the film (Figure 42). In other words, films sputtered within Oxygen rich ambient had fewer neutral and ionized Zn atoms. The lower carrier concentration of these films could not produce drastic improvement in free carrier mobility because ionized impurity scattering is not a dominant transport mechanism in the lightly doped polycrystalline films [chapter 5.1.1]. The damaging effects of Oxygen bombardment may also be a factor preventing the

enhancement in mobility, when sputtered within the higher Oxygen concentration [48]. In order to improve the electrical properties of these films, we annealed them for 45 minutes in Ar at 325°c.

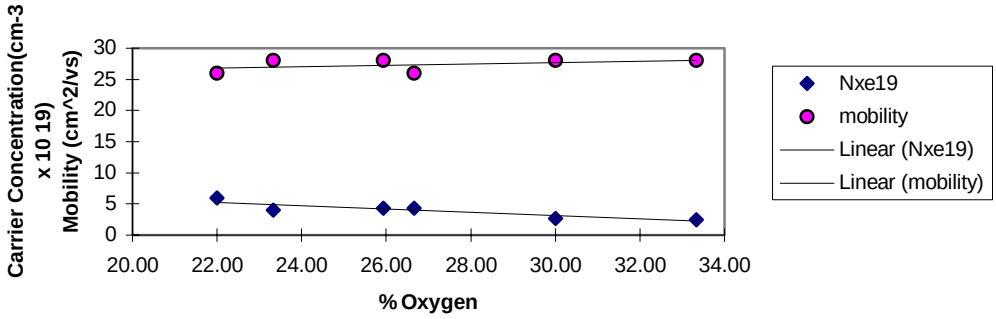

Figure 40 Carrier concentration and mobility of undoped ZnO as a function of oxygen content of the sputtering ambient at T = 200°c

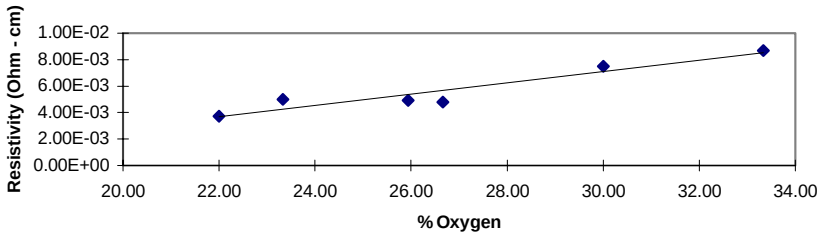

Figure 41 Resistivity of the undoped ZnO as a function of Oxygen content of the ambient

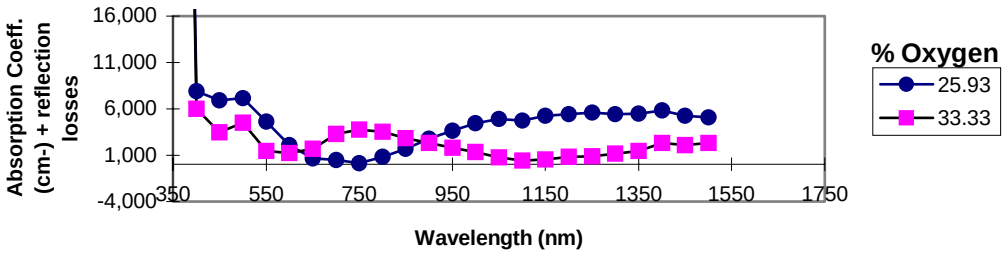

Figure 42 Absorption coefficient of an undoped ZnO films vs. wavelength for the films sputtered at 25.93% and 33.33% Oxygen concentration

As shown in Figure 44 and Figure 45, all annealed films showed decrease in carrier concentration and increase in the mobility. The resistance of all ZnO films was increased after the heat treatment (Figure 43). The improvement of electrical mobility was prominent for films sputtered in an Oxygen rich ambient. The mobility increased from 28 cm^2 v-s to 30 cm^2 v-s and carrier concentration decreased by a factor of two for the films sputtered with lower oxygen concentration (below 26%). Whereas, films sputtered with higher Oxygen concentration (33%) showed an increment of 10 cm^2 v-s in the mobility. Carrier concentration decreased by an order of a magnitude for these films. In other words, films sputtered with higher Oxygen concentration showed a significant decrement in carrier concentration and improvement in the electrical mobility when annealed. This can be attributed to the transfusion of Oxygen into the Oxygen deficient sites of the microstructure. As these films were annealed in Oxygen free ambient, such chemisorption of oxygen was negligible from the surface of the film. The decrease in carrier concentration can be due to the chemisorption of Oxygen, which was trapped at defects such as grain boundaries [49,50,46]. Films sputtered at higher Oxygen concentration had more Oxygen trapped at defect sites, which resulted in better stoichiometric films when annealed [28].

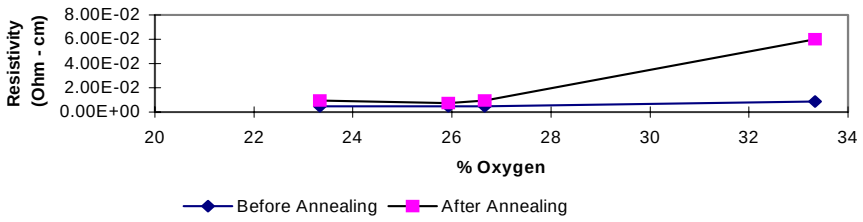

Figure 43 Resistivity of undoped ZnO films vs. Oxygen content of the sputtering ambient, before and after the 325°c anneal

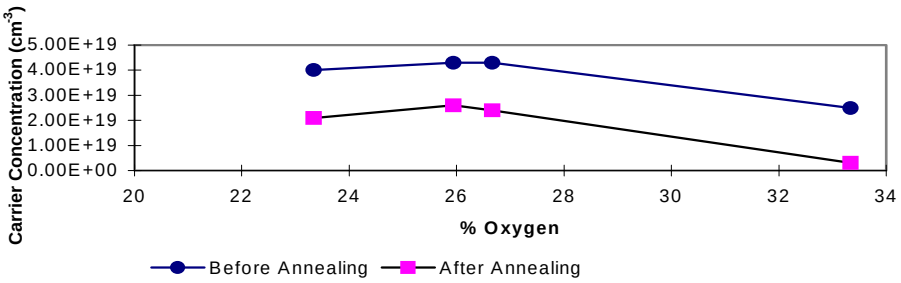

Figure 44 Carrier concentration of undoped ZnO films vs. Oxygen content of the sputtering ambient, before and after the 325°c anneal

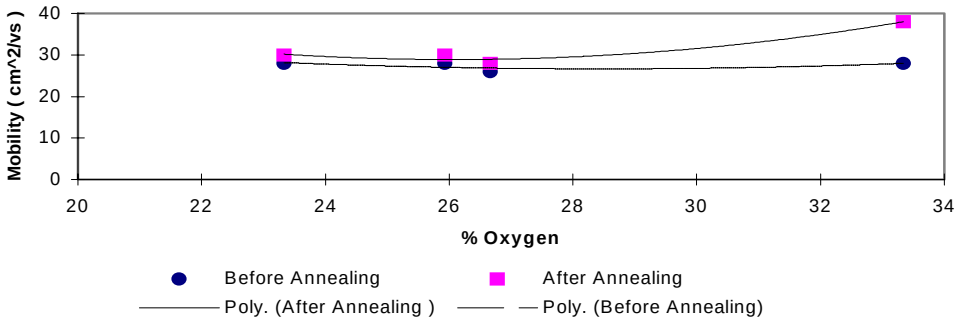

Figure 45 Mobility of undoped ZnO films vs. Oxygen content of the sputtering ambient, before and after the 325°c anneal

The decrease in carrier concentration after the heat treatment strongly suggested that the presence of interstitial/ trapped oxygen behaving as an acceptor was negligible in all films and that the carrier concentration of the undoped films sputtered during this work was mainly due to the oxygen vacancies or/and interstitial Zn ions.

The above observations imply that the higher Oxygen concentration in the sputtering ambient minimizes the Oxygen deficient sites in the deposited films. This results in lower free carrier concentrations. The improvement in mobility, after the heat treatment, can be attributed to less grain boundary scattering of the free carriers. Most likely, less scattering due to defects associated with trapped oxygen complexes.

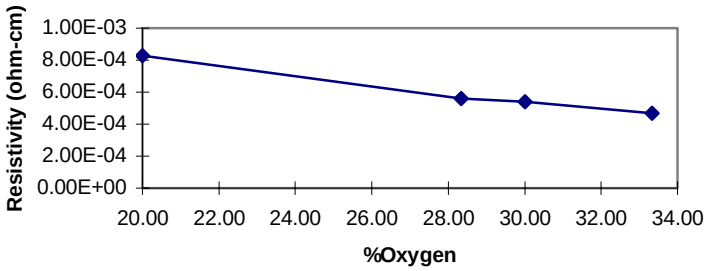

Figure 46 Resistivity of AZO vs. Oxygen content of the sputtering ambient

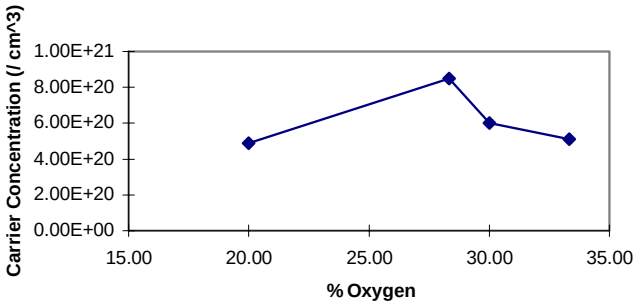

Figure 47 Carrier concentration of AZO vs. Oxygen content of the sputtering ambient

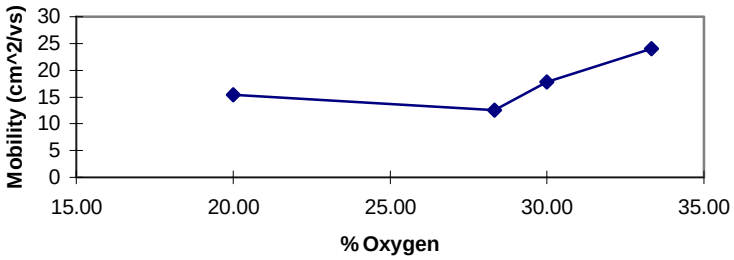

Figure 48 Mobility of AZO vs. Oxygen content of the sputtering ambient

Figure 46, Figure 47 and Figure 48 shows the electrical properties of the Al doped ZnO films. Typical carrier concentration of the doped films was in the range of 10^{20} $cm^{-3,}$ which was 10 times higher than the value for undoped films. In such a range, it is

unlikely that the significant influence of intrinsic carrier concentration on the total free carrier concentration can be observed. Thus the decrease in carrier concentration from 8.5 X 10^{20} to 5.10 X 10^{20}, when sputtered within the Oxygen rich ambient, can be attributed to the reduced dopant efficiency. The resistively of Al increases significantly due to oxidation even when it is evaporated in oxygen [43 14-347SP]. It is reasonable to accept that sputtered Al goes into a film as a partially or fully passivated oxide when deposited in an Oxygen rich ambient. Doped films sputtered in 42% Oxygen showed resistivity in the range of 10^{2} ohm-cm, which was comparable with the resistivity of undoped ZnO films. This observation indicates the presence of Al as an oxide within the film when sputtered in an oxygen rich ambient.

The mobility of the free carriers increased by the factor of two when sputtered in the Oxygen rich ambient. Less scattering of free electrons by ionized impurities can be a major factor responsible for such improvement.

The peak for Al and its oxides had not been detected by XRD measurement due to the very small amount of the dopant concentration (~ 0.60%).

The degradation of dopant efficiency prevented us from using Oxygen concentrations more than 35% within our experimental setup.

5.3.4 Effect of Substrate Temperature

Microstructure of reactively sputtered film is highly susceptible to the substrate temperature [12]. Consequently, Optical and electrical properties of the sputtered films showed strong dependence on the substrate temperature. ZnO deposited during this work was intended to be used on the substrate-configured solar cell. It was necessary to deposit the window layer at the substrate temperature that was safe enough to retain properties of the underlying material. The effect of substrate temperature was studied in order to establish the lowest possible temperature at which, reasonable optical and electrical properties can be achieved. The range of temperature was confined to be from room temperature to 350ºc.

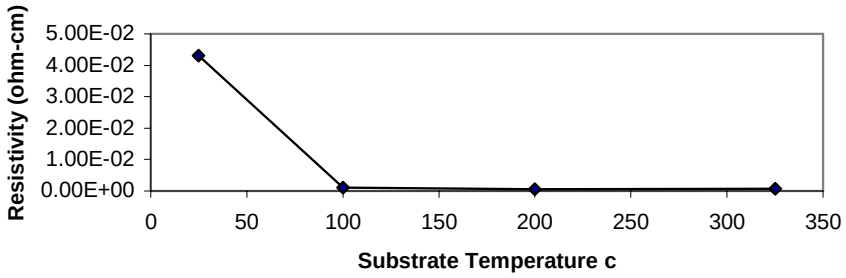

Figure 49 Resistivity vs. substrate temperature for AZO in zone D

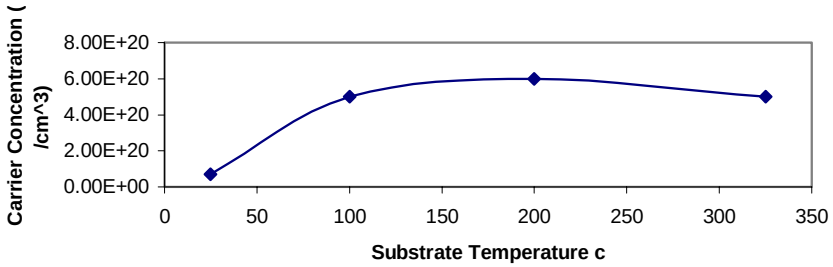

Figure 50 Carrier concentration vs. substrate temperature for AZO in zone D

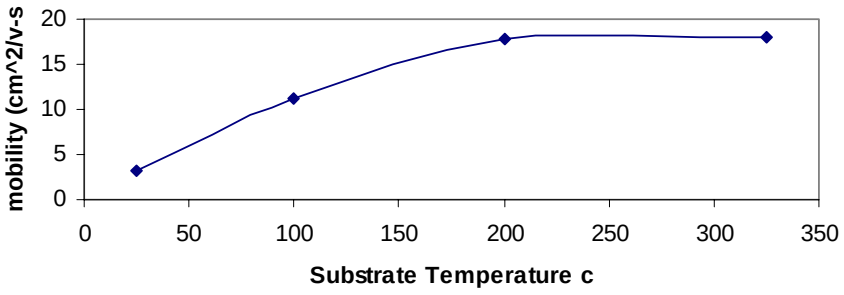

Figure 51 Mobility vs. substrate temperature for AZO in zone D

As shown in Figure 49, resistivity of the Al doped film in region D decreased when deposition temperature was increased from room temperature to 100ºc. Low resistivity in the range of $5x10^{-4}$ was independent of substrate temperature between 200ºc and 325ºc. Such behavior has also been noted by other groups [51]. Figure 50 and Figure 51 shows the electrical properties of the film deposited in zone D. This zone was practically free from the bombardment damages at selected sputtering parameters. Carrier concentration and mobility significantly increased when substrate heating was provided (Figure 50 and Figure 51). Consequently, the resistivity of the film dropped from 4.3 x 10-2 ohm-cm to 1.09 x 10-3 ohm-cm. The increase in mobility with the increase in temperature (up to 200°c) was due to improved microstructure and crystallinity of the film [51].

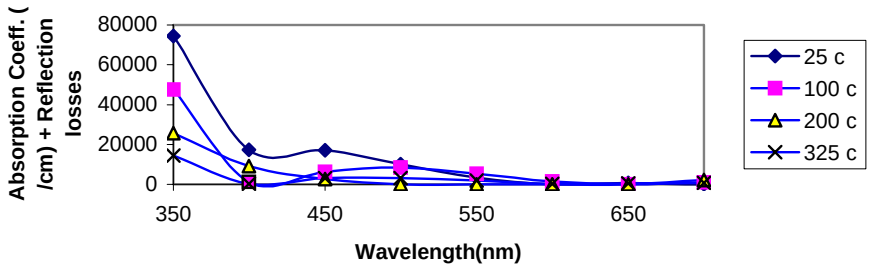

Figure 52 Absorption coefficient of the AZO films sputtered at different substrate temperatures (visible range)

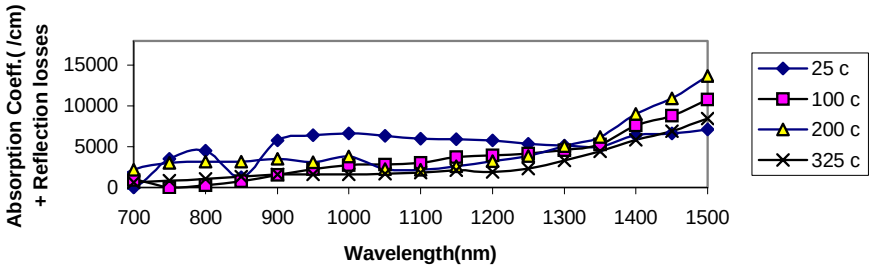

Figure 53 Absorption coefficient of the AZO films sputtered at different substrate temperatures (IR range)

Table 11 shows the electrical properties of undoped ZnO films. Carrier concentration of these films decreased when the substrate temperature was elevated. The decrease in carrier concentration indicated better stochiometry of the film. Al doped as well as undoped films became more transparent, especially in the visible spectrum of light, when substrate temperature was elevated (Figure 52 and Figure 53).

Analysis of the electrical and optical properties of these films suggested that substrate temperature improved stochiometry and crystallinity of the film [53]. The observation that films prepared at higher substrate temperature were less Oxygen deficient confirmed that substrate temperature stimulates oxidation of the film on the substrate [52 pg.59].

Table 11 Comparison of carrier concentration and mobility of the undoped ZnO films sputtered at different substrate temperatures

Substrate Temperature (°c)	Carrier Concentration (cm^{-3})	Mobility (cm^2/vs)
25	9.2×10^{19}	6
100	5.7×10^{19}	30
200	5.10×10^{19}	35
325	8×10^{18}	36

Table 12 Comparison of carrier concentration and mobility of an Al doped ZnO film before and after annealing in Ar at 200°c

Deposition Temperature	Carrier Concentration (cm^{-3})		Mobility (cm^2/Vsec)	
	Before Annealing	After Annealing	Before Annealing	After Annealing
25°c	7.0 E 19	4.40 E 20	1.8	6.20
100°c	5.0 E 20	5.5 E 20	11.2	12.6

Table 13 Electrical properties of an Al doped ZnO film Deposited at 200°c

Deposition Temperature	Carrier Concentration (cm^{-3})	Mobility (cm^2/Vsec)
200°c	6.20 e20	17.8

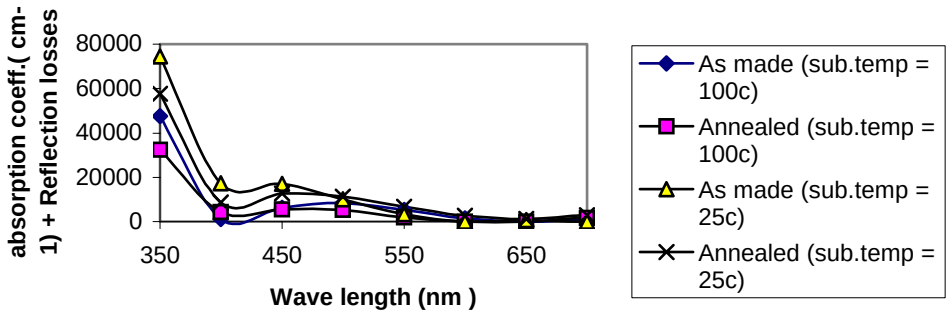

Figure 54 Effects of 200°c anneal on the absorption coefficient of the films deposited at different substrate temperatures (visible range)

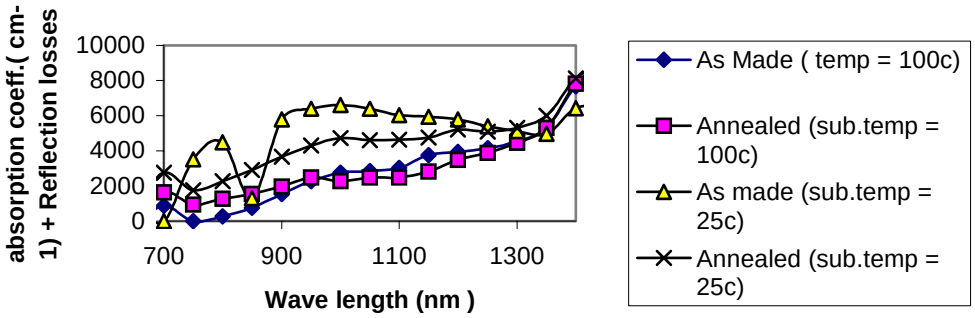

Figure 55 Effects of 200°c anneal on the absorption coefficient of the films deposited at different substrate temperatures (IR range)

Films sputtered at 25ºc and 100ºc were annealed at 200ºc in Ar ambient for 45 minutes to study the effect of heat treatment on these films. As shown in Figure 54 and Figure 55, transmission of the film was slightly improved after the heat treatment. From Table 12, it is clear that mobility and dopant efficiency of the film were enhanced due to the heat treatment.

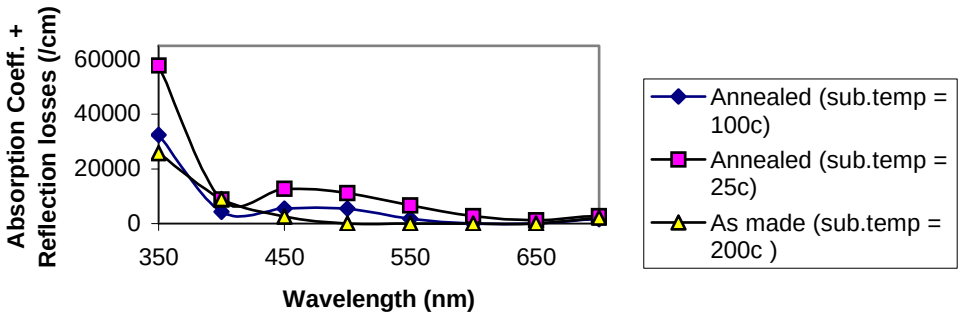

Figure 56 Absorption coefficient of the films sputtered at 100°c and 25°c (after the 200°c anneal) is compared with that of AZO sputtered at 200°c substrate temperature (visible range)

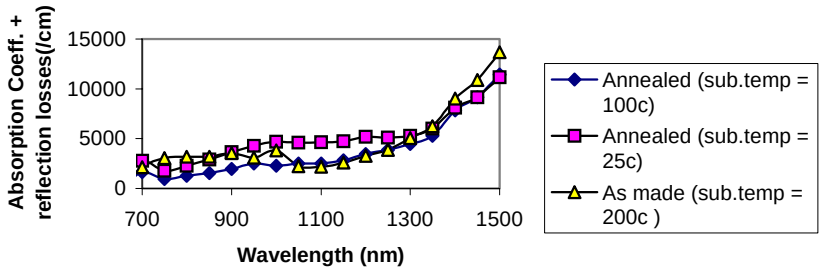

Figure 57 Absorption coefficient of the films sputtered at 100°c and 25°c (after the 200°c anneal) is compared with that of AZO sputtered at 200°c substrate temperature (IR range)

Optical properties of the annealed films and a film deposited at 200°c are compared in Figure 56 and Figure 57. The electrical properties of a film prepared at 200°c are listed in Table 13. It is clear that the electrical and optical properties of the annealed films could not reach the values for the film sputtered at 200ºc. Annealing temperature was not sufficient enough to improve the crystallinity of the film and XRD analysis could not detect any significant change after the heat treatment. The enhancement of optical and electrical properties can solely attributed to the improvement of the stochiometry and defect structure due to the heat treatment.

Table 14 Electrical properties of the AZO film deposited at room temperature and annealed in Oxygen and Ar ambient at 200°c for 45 min

	Deposited at 25°c	Annealed at 200°c in 100%Ar	Annealed at 200°c in 50% O_2 +50%Ar
	Step 0	Step 1	Step 2
Carrier Concentration (cm^{-3})	6.0E 19	3.1 E20	3.0 E 20
Mobility (cm^2/V sec)	2.2	6.8	8.2
Absorption coeff (/cm) at 500nm	10050	11830	12460

AZO sputtered at room temperature was annealed at 200°c in the presence of Oxygen to promote chamiabsorption of Oxygen from the ambient. Table 14 shows the electrical and optical properties of these films. It is clear from the observations that an annealing temperature of 200°c was not sufficient enough to initiate significant chamiabsorption of the Oxygen from the surface of a film. The improvement of electrical properties was entirely temperature enhanced.

5.4 Proposed Sputtering Parameters for ZnO

Deposited ZnO films are categorized into three groups according to their optical and electrical properties (Figure 58 and Figure 59). Films belonging to first group are opaque and conductive. Such films are characterized as a mixture of Zinc and Zinc oxide. These films are prepared at lower substrate temperature or/and higher sputtering voltages with less oxygen flow rates. Films of the third group have a composition close to stoichiometry of ZnO and are transparent and non-conductive. Films of this group are most suitable for the resistive layer of zinc oxide on solar cells. Group two films have intermediate properties. Transparent as well as conductive films fall in this category.

Undoped films sputtered at lower voltages (440 V), moderate temperature (200°c) and higher oxygen concentration (~50%) can be placed in category three. These films showed resistivity more than 10 ohm-cm and average absorption coefficient in the range of 1600 cm^{-1}. Change in the electrical resistivity was not detected after the 325°c anneal. These stoichiomentric films showed good thermal stability.

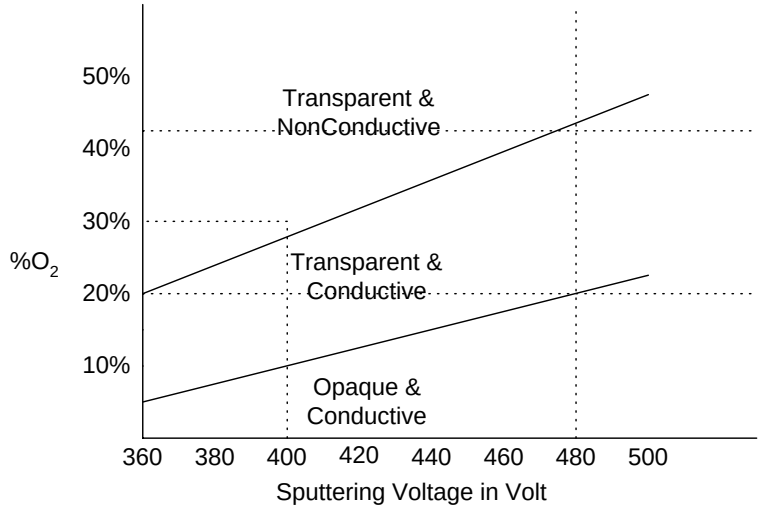

Figure 58 Effect of oxygen concentration and sputtering voltage on the electrical and optical properties of ZnO

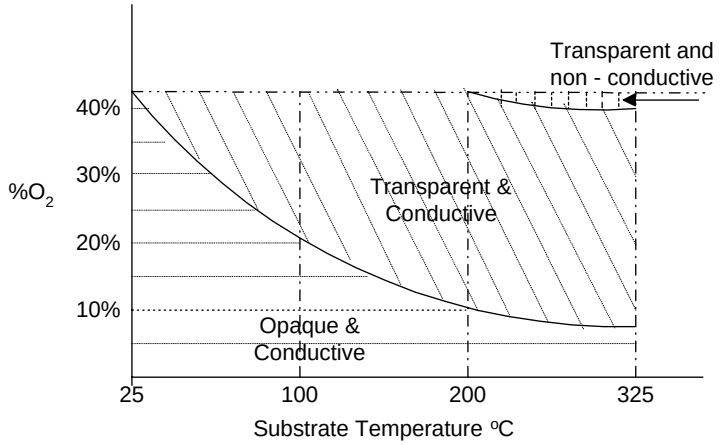

Figure 59 Effect of Oxygen concentration and the substrate temperature on the electrical and optical properties of ZnO

Transparent and non-conductive ZnO (category 3) should result in an ideal conductive transparent film when doped with Aluminum. As shown in Figure 58 and Figure 59, such film can be deposited with higher substrate temperature or within the O_2 rich ambient. An upper limit of the substrate temperature was set to 350ºc as AZO films studied during this work were intended to be used on CIS solar cells. In this range of temperatures, stochiometric film can be deposited either with lower sputtering voltages or with higher oxygen concentrations. As dopant effect of Al is achieved around 440 V, the only way to sputter doped films in category three is to use at least 40% oxygen concentration in the sputtering ambient. On the other hand, sputtered aluminum goes into a film as a passivated oxide if sputtered with oxygen concentration higher than 29%. Due to these practical limitations, all Al doped films sputtered during this work fall in the group two categories.

The optimum combination of optical and electrical properties was repetitively shown by the films sputtered with 480 Volt, 3 mTorr pressure, 30% O_2 concentration and 325ºc substrate temperature. Spatial distribution of resistivity and deposition rate with respect to the target position are shown in Figure 60. Figure 61 shows optical properties of this film. The best-achieved properties of reactively sputtered AZO reported by other groups are comparable with these results [47,12].

Zone	A	B	C	D	E
Deposition Rate	2.56ºA/s	1.71ºA/s	1.23ºA/s	0.85ºA/s	.53ºA/s

Resistivity:

A	B	C	D	E
0.63	0.45	0.50	0.55	0.71
1.60	0.44	0.42	0.44	0.60
0.90	0.47	0.48	0.54	0.66
0.59	0.48	0.56	0.67	0.68
0.48	0.52	0.64	0.75	0.83

Figure 60 Resistivity (x10^{-3} ohm-cm) of AZO on 10 cm x10cm substrate relative to the location of sputtering source

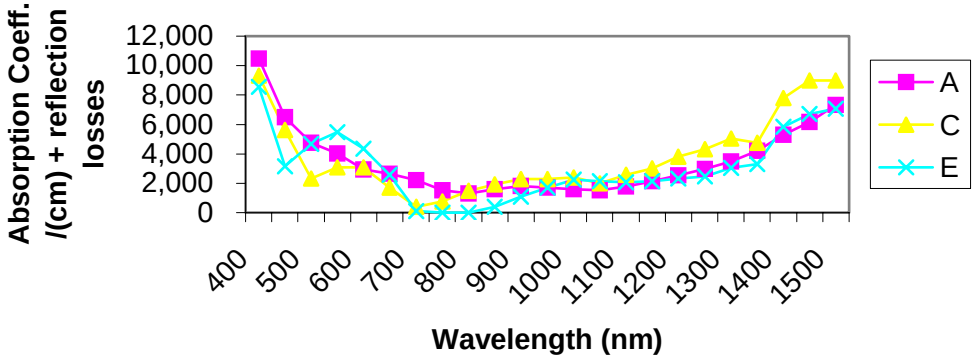

Figure 61 Optical properties of AZO in different sputtering zones

5.5 Comparison between AZO Sputtered from Oxide Target and Metal Target

ZnO window layers have been successfully sputtered form Oxide targets with the RF sputtering technique in the USF semiconductor lab. Properties of reactively sputtered ZnO were compared with such films in order to examine its prospective for CIS solar cell.

The window layer of CIS solar cells has been sputtered from a Zinc Oxide target at 100°c. Electrical properties of a typical film are shown in Table 15. Properties of a film sputtered from a zinc target using reactive dc sputtering are listed in Table 16. In order to make the fair comparison, both films were deposited at 100°c using similar experimental setups.

Faster deposition rate is the main advantage of DC sputtering. Lower heat conductivity and heat dissipation in Oxide targets puts an upper limit to RF sputtering power. On the other hand, metal targets withstand higher power densities without heat-induced damages. Sputtering power as high as 200 W was used without damaging the Zn target during this study. We can probably go to kilowatts in power without heating the Zn target. Whereas, the safe power limit for a ZnO target with the same experimental set up was under 100W. As deposition rate is directly proportional to the sputtering power, higher growth rate was achievable with the DC sputtering technique.

The Films compared in Tables 15 and 16 were deposited with sputtering power under 100W. When sputtered with the same electrical power, growth of the film was faster with the Zn metal target. This can be attributed to the difference in the sputtering yields of both the materials. Since the binding energy of ZnO is greater than that of the Zn, the sputtering yield of Zn is higher than its oxide [26]. In other words, the higher deposition rate of a film sputtered from a Zn target can be attributed to the fact that oxides sputter much more slowly than a pure metal.

Table 15 Electrical properties of an Al doped ZnO film sputtered by RF sputtering

Deposition Rate (Å/s)

A	B	C	D	E
1.22	1.01	0.76	0.58	0.41

Resistivity (x $1e^{-3}$ Ohm-cm)

8.3	2.4	1.4	1.9	4.3
24	2.8	1.2	1.7	4.7
89	4.2	1.2	1.5	4.5
90	5.3	1.2	1.6	3.7
93	4.5	1.2	1.6	3.9
34	2.9	1.2	1.8	4.1
15	2.2	1.2	1.9	4.7
8.2	1.8	1.2	2.1	5.7

Table 16 Electrical properties of Al doped ZnO film sputtered by DC reactive sputtering

Deposition Rate (Å /s)

A	B	C	D	E
1.65	1.52	1.07	0.69	0.55

Resistivity (x 1e-3 Ohm-cm)

1.7	1.2	1.5	1.6	1.3
2.7	1.3	0.97	0.92	1.1
4.0	1.6	0.94	0.84	1.3
6.2	1.7	0.94	0.80	1.0
7.7	1.7	0.97	0.81	1.0
7.6	2.7	0.45	0.83	.98
4.6	2.0	0.94	0.81	1.0
3.3	1.8	0.96	0.94	1.0

Spatial distribution of electrical resistivity was uniform when sputtered with reactive sputtering (Table 15 and 16). Positional dependence of resistivity of AZO sputtered from the oxide target has been attributed to the bombardment of highly energetic oxygen species [53,54]. The origin of these high-energy Oxygen species can be the oxygen atoms in the oxide target [48]. The flux of high-energy neutrals is smaller for Zn metal targets than for Oxides target [40]. Moreover, the ratio of atomic to molecular oxygen was reported to be higher in the case of the RF sputtering mode [55]. Less position dependence of resistivity, seen in DC reactively sputtered films suggests less high-energy oxygen bombardment on the grounded substrate. As mentioned previously (chapter 5.5), most of the Al doped films were sputtered in the Oxygen deprived sputtering ambient. Less Oxygen concentration in the sputtering ambient might also have prevented the damage caused by high-energy Oxygen species, which resulted in less spatial variation in the resistivity of the reactively sputtered films.

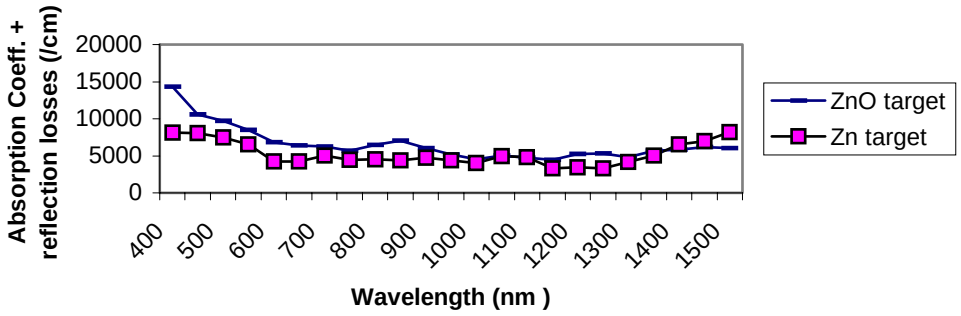

Figure 62 Comparison of the optical properties of AZO films sputtered from Zn and ZnO targets

AZO Films sputtered with reactive sputtering were more conductive than the RF sputtered films. Optical parameters of both films are also comparable (Figure 62). More flexibility of sputtering parameters offered by reactive sputtering provided a large

spectrum of deposition combinations. The best combinations of electrical and optical properties were achieved with DC reactive sputtering.

Compared to the metal target, control of film stoichiometry was easier when the Oxide target was sputtered. Undoped films sputtered from the oxide target often showed high resistivity and were less metal rich. Films must be sputtered in high Oxygen concentration and with slower deposition rate from the Zn target to achieve similar properties. Use of an Oxide target is recommended over a metal target for undoped ZnO deposition.

Metal targets are cheaper than Oxide targets. Besides, a variety of compound metal targets can be easily fabricated. Faster deposition rate and less positional dependence of the properties result in high throughput when a Zn target is used. Moreover, the high cost of RF generators, matchboxes and wavelength interference makes the RF sputtering technique more costly [8].

Sputtering from a Zn target is less simplified but more economic. DC reactive sputtering offers better flexibility to establish optimum combinations of process parameters. Such flexibility increases the opportunity of achieving the best combinations of desirable properties for window layer ZnO.

5.6 Performance of Reactively Sputtered ZnO Window Layers on CIS Solar Cells

5.6.1 CIS/CdS/ZnO Devices

Deposition of ZnO window layers is the final step of CIS solar cell fabrication. The process of window layer deposition should not only grow a transparent and conductive oxide, but should also conserve the properties of the underlying material.

The critical parameter for preparation of the front contact is the substrate temperature. The interdiffusion of Cd into Cu ternaries has been reported at temperature greater than 300°c. A substrate temperature above 200°c causes Interdiffusion of Se into S [8]. The ZnO window layer must be prepared under 200°c to prevent the adverse effects on the underlying CIS layer.

To start with both, undoped and doped, layers of ZnO were sputtered at 200ºc. All of the devices completed with this window layer did not show diode characteristics during IV measurement. In other words, the devices were shorted.

These shorted devices suggested that other than inter diffusion of Sulfur and Selenium, The reactive nature of the ZnO deposition could also be a decisive parameter for the substrate temperature. To study the effect of sputtering ambient on the performance of solar cells, CIS solar cells with conventional RF sputtered ZnO were annealed at 200ºc in Ar and O_2 for 45 min.

Table 17 (h19-23 H17-08): Diode properties of a CIS solar cell after 200°c anneal in Ar and O_2 ambient

	Annealed in Ar at 200ºc	Annealed in 75%Ar 25% O_2 at 200ºc
Voc Before Annealing	433mV	419mV
Voc After Annealing	420mV	383mV
Jsc before annealing	39.2 mA/cm^2	36.1 mA/cm^2
Jsc after annealing	40.5 mA/cm^2	42.9 mA/cm^2

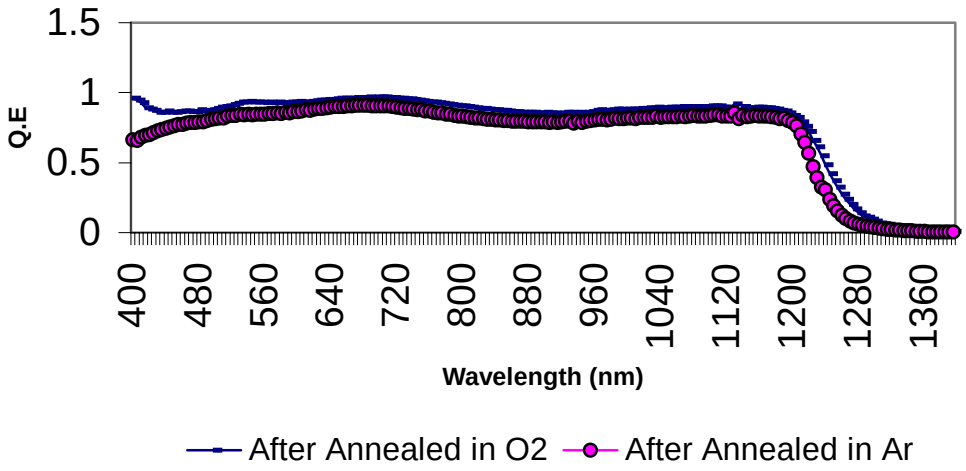

Figure 63 Comparison of the spectral responses of a cell annealed in Oxygen and Ar ambient

As shown in Table 17, a 9 % decrease in Voc was observed when the film was annealed in 75% Ar and 25% oxygen, whereas the decrease in Voc was 3% when annealed in pure Ar atmosphere. This suggested that the CdS layers in these devices were not thick enough to protect diffusion of O_2 into the CIS absorber layer at 200ºc [j.Kessler 1996]. Spectral response for these devices is shown in Figure 63.

In order to minimize the adverse effect of Oxygen, we tried to deposit window layers at lower substrate temperatures. Doped and undoped layers of ZnO were sputtered at room

temperature on CIS absorption layer. The completed device was then annealed in Ar at 200°c for 45 minutes in order to improve the electrical and optical properties of the ZnO layer. Open circuit voltages of this device and reference device are compared in Table 18.

Table 18 (h19-23, h19 r23 get h19) Diode properties of the device fabricated with reactive ZnO and the reference device. Reactive ZnO was sputtered at room temperature and annealed in Ar ambient at 200°c for 45 min

	Reference cell with RF sputtered ZnO	Cell with reactively sputtered ZnO
Voc	433mV	400 mV
Jsc	39.2 mA/cm^2	28.2 mA/cm^2
FF	60%	56%
% EFF	10%	6.2%

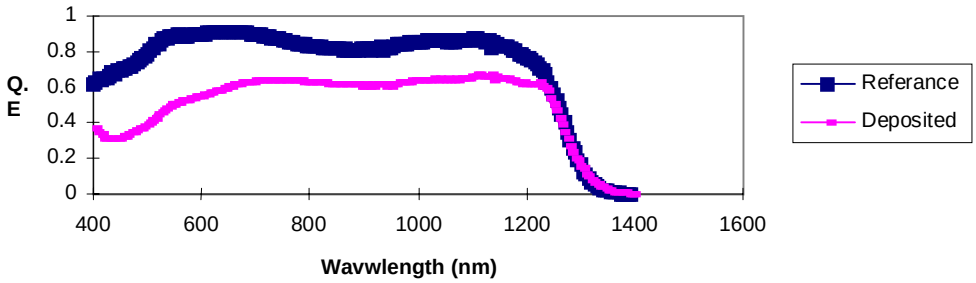

Figure 64 Spectral response of the reference device and a device fabricated with a reactive ZnO window layer. The reactive ZnO layer was deposited at room temperature and annealed in Ar ambient

As shown in Figure 64, the current density of the device completed with reactively sputtered ZnO was 28.2 mA/cm^2 , which was 10 mA/cm^2 less than the value for the reference cell. Lower transmission (70 %) and higher sheet resistance (36 ohm-cm^2) of DC sputtered ZnO were responsible for poor performance of the device. This device

suggested that ZnO should be sputtered at least at 100ºc when used as a transparent conductive oxide.

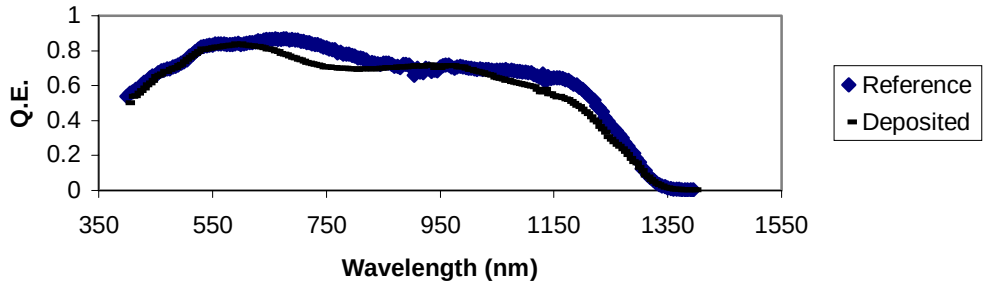

Figure 65 Spectral response of the reference device and a device fabricated with a reactive ZnO window layer. The undoped ZnO was sputtered at room temperature. The AZO was sputtered at 100°c

Table 19 (7h20-2r,h20-07) Diode properties of a reference device and a device with DC sputtered ZnO. Undoped ZnO was sputtered at room temperature and AZO was sputtered at 100°c

	Reference Cell with RF Sputtered ZnO	Cell with Reactively Sputtered ZnO
Voc	367mV	376mV
Jse	35.9 mA/cm^2	33.6 mA/cm^2
FF	56%	57%
% Eff	7.3%	7.2%
Duration of Window layer deposition	~ 2hrs 30 min	~ 1 hrs 30 min
Thickness of I-ZnO layer	500Å	900 Å
Thickness of AZO	5000 Å	3000 Å

In another set of experiments, undoped ZnO was sputtered at room temperature to avoid the exposure of under lying CdS to Oxygen at high temperature. A 2000ºA thick Al doped ZnO layer was reactively sputtered at 100ºc on the undoped ZnO layer.

Performance of this device and the reference device were practically identical (Table 19). Spectral response of a cell with a reactively sputtered ZnO window layer is compared with that of a RF sputtered ZnO window layer in Figure 65.

The deposition of the reactively sputtered ZnO was faster than RF sputtered ZnO. Moreover, a thinner layer of doped ZnO offered acceptable surface conductivity. Use of RF sputtered ZnO was not only costly but also time consuming compared to the use of reactively sputtered ZnO.

There is enough room for other process combinations, which can further improve the performance of CIS solar cells with the reactively sputtered ZnO window layer. These results encourage us to believe that reactively sputtered ZnO can not only replace RF sputtered ZnO window layer on CIS solar cell but also be proven superior to the conventional window layer.

5.6.2 Direct CIS/ZnO Devices

Before the ZnO deposition, a CdS buffer layer is deposited using a chemical bath deposition (CBD) technique. Device fabrication, without a wet chemical step of the highly toxic CdS deposition, is an on going investigation. Many groups have reported the significance of the CdS layer in preventing the CIS layer from the exposure of oxygen during the front contact formation [3,6,8]. Some of the groups have successfully fabricated Cd free CIS solar cells with 10.5% efficiency [6]. These reports suggested the use of a non-O_2 containing RF plasma process. Addition of Oxygen in the sputtering ambient severely degraded the performance of the Cd free cell [6,3]. We tried to explore the effect of the reactive nature of DC sputtering on the Cd free solar cell. Reactively

sputtered ZnO was deposited on the CIS layer, without CdS deposition to examine the future of this deposition technique for Cadmium free devices.

Deposition of intrinsic ZnO is the most critical process in Cd free devices, as the undoped ZnO layer is directly deposited on the absorption layer. This layer was deposited with reactive sputtering, whereas the doped ZnO layer was deposited with standard RF sputtering. The undoped ZnO layer was sputtered at room temperature with 33% oxygen concentration. Doped ZnO was sputtered using conventional RF sputtering at 100ºc. Table 20 compares the device properties of all reactively sputtered ZnO junction devices with the literature results.

Table 20 (H34 14/H34) Diode properties of CIS/ZnO devices compared with literature results

	CIS/ZnO (Literature)[28]	CIS/ZnO (USF)
Voc (mV)	390	350
Jsc (mA/cm$^{2)}$	34.6	32.1
FF	39%	35%

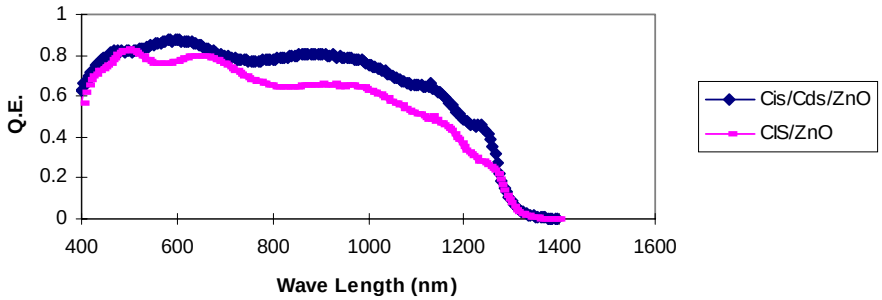

Figure 66 Spectral response of a CIS/CdS/ZnO device and a CIS/CdS device

Spectral responses of these devices are compared in (Figure 66). The CdS free cell showed 350 mV Voc and 32.1 mA/ cm^2 of Jsc. During the study, the Voc's of all Cd free devices were within 10-20% of the values for the conventional cells. However, Jsc was affected most when the Cds layer was eliminated. Almost 10% loss in Jsc was seen in the spectral response (Figure 66). Many devices showed shunting in the dark IV curve. Fill factor was also low compared to CdS control devices. Low open circuit voltage and fill `factor degraded the efficiency of this device. Other groups have also noticed such degradation in CdS free cells with RF sputtered ZnO window layers [6].

Results of this experiment encourage us to conclude that despite the use of oxygen in the sputtering ambient, reactive sputtering can still be a candidate for direct CIS/ZnO devices. Less damage caused by energetic oxygen spices and O_2 deficient plasma processes of DC sputtering may favor the endeavor of Cd free fabrications.

CHAPTER 6 CONCLUSION

This work demonstrated that the reactive sputtering technique could be successfully used for window layer deposition on Cu(In,Ga)Se_2 solar cells. Films sputtered with reactive sputtering showed better electrical and optical properties compared to the films sputtered with conventional RF sputtering. Reactive sputtering technique was less time consuming and cheaper compared to the RF sputtering technique.

Conductivity of the undoped ZnO was a result of oxygen vacancies and excess Zn. Typical carrier concentration of such films was 5 x 10^{19} cm^{-3}. Mobility of carriers in undoped ZnO showed dependence solely on grain boundary scattering and defect-induced scattering. Unlike Al doped ZnO; these films did not show a consistent relationship between carrier concentration and mobility. Typical carrier concentration of Al Doped ZnO was 5x 10^{20} cm^{-3}. Mobility of these films showed dependence on carrier concentration as well as on microstructure of the film.

Undoped films sputtered at lower voltages (440 v), moderate temperature (200°c) and higher oxygen concentration (~50%) were stoichiometric and suitable for the buffer layer application. These films showed resistivity more than 10 ohm-cm and average absorption coefficient in the range of 1600 cm^{-1}. These ZnO films were stable at higher temperatures. The optimum combination of optical and electrical properties were

repetitively shown by the AZO films sputtered with 480 Volt, 3 mTorr pressure, 30% oxygen concentration and 325°c substrate temperature.

Growth of the film was more temperature dependent when sufficient flux of Zn and Oxygen was available near the substrate surface. The film sputtered at lower substrate temperature was inferior. The heat treatment improved the optical and electrical properties of such films. Electrical and optical properties of the film sputtered at higher temperature could not be achieved by annealing the film sputtered at lower temperature. The minimum temperature, which could produce reasonable electrical and optical properties, was 100°c.

Oxygen in the sputtering ambient degraded the absorbent layer during front contact preparation. The adverse effect of oxygen was minimized when the undoped layer was deposited at room temperature. Performance of devices prepared with such procedures was comparable with devices fabricated with a conventional ZnO layer.

The elimination of a CdS buffer layer degraded the Fill Factor and Jsc of the device. However, we were successful in improving Voc. Results of this study encouraged us to conclude that despite the use of oxygen in the sputtering ambient, reactive sputtering can still be a candidate for direct CIS/ZnO devices.

REFERENCES

1. J.R. Tuttle, J.S. Ward, A Duda , T.A.Bernes, M.A.Contretas, K.R,Ramanathan,A.L. Tennant,J.Keane, E.Dcole, K.Emery and R.Noufi " *The Performance of Cu(InGa)Se_2 Based Solar Cells in Conventional and Concentrator applications*", Proceeding of the 1996 spring MRS meeting , San Fran, Ca, 1996.

2. K.Zweible, " *Progress in Photovoltaics*", Special issue on thin films (1995).

3. J.Kessler, S.Wiedeman, L.Russel, J. Fogleboch, S.Skibo, R.Arya, and D.Carlson, " *Front Contact Optimization for Cu(InGa)Se_2 (SUB) Modules*", 1996 IEEE 25th PVSC , May 1996 , Washington D.C.

4. J.Kessler, K.O.Velthaus, M.Rouck, R.Laichinger, H.W.Schock, D.Lincot, R.Ortega Borges and J.Vedel. Proc 6th International PVSEC , New Delhi, Oxfprd and IBH Publ., New Delhi 1992 p.1005.

5. J. Hedstrom, M.Bodegard, A.Kylner, L.Stolt, D.Heriskos, M. Ruch and H.W.Shock IEEE 1993.

6. J.Kessler, M.Ruckh, D.Hariskos, U.Ruhle, R.Menner and H.W.Schock, "Interface Engineering Between *Cu(InGa)Se_2* and ZnO" IEEE 1993.

7. R.W.Birkmire, B.E.McCandles, W.N.Shafarman and R.D. Varrin, Jr.Proc 9th EC PVSEC, Freiburg Kluwer, Dordrect (1989) p.134.

8. M.Ruckh, D.Hariskot, U.Ruhle and H.W.Schock. " Application of ZnO in *Cu(InGa)Se_2* Solar Cells" , 1996 IEEE 25th PVSC , May, 1996, Washington D.C.

9. Physics of Semiconductor Devices by S.M.Sze.

10. Erginsoy C 1950 Phys.Re 79 1013 (Semiconductor Thin Films).

11. Johnson VA and Lark, Horovitz K 1947 Phys. Rev 71 – 374 (Semiconductor Thin Films).

12. S.Zafar, C.S.Ferekides and D.Morel. *"Characterization and Analysis of ZnO Al Deposited by Reactive Magnetron Sputtering"*, J.Vac.Sci.Technol A13 (4) 1995.

13. Solar Cell Device Physics by Stephen J. Fonash.

14. Seto JYW 1975 J.Appl.Phy 46 – pg 5247 (Semiconductor Thin Films).

15. Padovani FA and Stratton R, 1966 Solid State Electron 9 pg 695 (Semiconductor Thin Films).

16. Crovell CR and Rideout VL 1969 Solid State Electron 12 pg 89 (Semiconductor This Files).

17. Semiconducting Transparent Thin Films by H.L.Hartangel, A.L.Dawar, A.K.Jain and C Jagadish.

18. Roth AP and Williams DF 1981 J. Appl Phys. 52 pg86685.[17].

19. Sinois F, Leiji MV and Hoogendoorn CJ 1979 Solar Energy Mater 1 pg 221.

20. Smith RA 1978 Semiconductors (Cambridge, Cambridge University Press) pg 294.[17].

21. Krokoszinski HJ and Oesterlein R1990 Thin Solid Films 187 pg179 , [17].

22. Burstein E 1954 Phys. Rev 93 Pg632, [17].

23. Moss TS 1964 Proc. Phys.Soc B67 Pg 755, [17].

24. Sarkar A, Ghosh S, Chaudhri S and Pal AK 1991, Thin Solid Films 204 pg 255, [17].

25. Minami T, Oshashi K, Takata S, Mouri T and Ogawa N , 1990 Thin Solid Films 193/194 Pg721.

26. Semiconductor Materials and Process Technology Handbook by G.E.McGuire , Noyes Publications 1988.

27. Zinc Oxide Rediscovered by Harvey Brown, The New Jersey Zinc Company 1957.

28. R.Bhatt, H.Shankernarayan, C.S.Ferkides and D.L.Morel , 26th IEEE Photovoltic Specialists Conference , 383 ,IEEE1997.

29. Chelikowasky JR 1977 Solid State Commun. 22 pg 361.

30. Hustson , Bul A.M. 1956 Phys.Soc.Series 2. Vol 1 , 381 , [27].

31. Hagemark KL and Chaccka LC 1975, J.Solid State Chem. 15 pg 261.

32. Gopel W and Lanoe U 1980 Phys.Rev B 22 pg 6447.

33. Akarussaman AF, Sharma GL and Malhotra LK 1985, Thin Solid Films 193/194.

34. Minami T, Sato H , Sonada T, Nato H and Takata S 1989 Thin Solid Fils 171 pg.307.

35. Hu J and Gordon R 1992 J.Appl.Physics 71 pg.880, [17].

36. Chi BH, Song JS, Yoon Kh 1990 Thin Solid Films 193/194 pg 712,[17].

37. Sarkar A, Ghosh S, Chudhari S and Pal AK 1991, Thin Solid Films 204/255.

38. Gary, J Amer, Ceramic Soc 1954, 37:534,[27].

39. Barns Jo, Leary Dj and Jordan AG 1980 J. Electrochem. Soc. 127 pg 1636 , [17]

40. S,B Krupanidhi and M.Sayer "Position and Pressure Echen ffects in RF Magnetron Reactibe Sputter Deposition of Piezoelectric Zinc Oxide", J.Appl.Phys, 56 pg 3308.

41. Wen S Chen , J.M. Stewart, R.A. Mieckelsen, W.E. Devaney and B.J. Stanbery " Research of Phlycrystalline This n Film $CuGaInSe_2$ Solar Cells ", Boeing defense and space group , final technical report for the period May 3rd 1991 through May21 , 1993.

42. Leja E, Budzynska K, Pisarkiewicz T and Stapinski T 1983 This Solid Films 100 pg.203.

43. Donaghy L.F. and Gerghty K.G. 1976 Thin Solid Films 38 pg.835.

44. Shinoki F and Itoh A 1975 , Appli. Phys. 46 pg.3381.

45. Tsuji N, Komiyama H and Tanaka L 1990 Japan . J. Appl. Phys 29 pg.835.

46. T.Minami, H.Nata and S.Takata "Highly Conductive and Transparent Aluminum Doped Zinc Oxide Thin Films Prepared by RF Magnetrone Sputtering, Japanese J. Apply.Phys 1984 23, pg L280.

47. Z.C. Jin, I.Hamberg and C.G.Granqivst, "Optical Properties of Sputter Deposited ZnO:Al Thisn Films", J.Appl.Phys. 1988 pf5117.

48. Kikuo Tominaga, Satoshi Iwamura, Yoshihiro Shinitani and Osamu Tada, "Energy Analysis of High Energy Neutral Atoms in The Sputtering of ZnO and $BatiO_3$ " , Japanese J. Appl. Phys. 1982, 21 pg 688.

49. T.Minami , H.Nato,S.Shooji and S.Takata , 1984 ,Thin Solid Films , 111, pg.167.

50. Schoenes J, Lanazawa K and Kay E 1977 J.Appl.Phys 48 pg.2537.

51. Minami T, Nato H and Takata S, 1985, Thin Solid Films 193/194.

52. Thin Film Process by Jhon Vossen and Werner Kern. Academic Press 1978.

53. T.Minami, H.Sato, H.Imamoto and S.Takata, "Substrate Temperature Dependence of Transparent Conducting Al Doped ZnO Thin Films Prepared by Magnetron Sputtering" J.Apl. Phys. 1992, 31, pg L257.

54. Yong Eui Lee and Jae Bin Lee " Microstructure Evolution and Preffered Orientation Changes of Radio Frequency Magnetron Sputtered ZnO Thin Films", J.Vac.Sci Technol.1996 A 14 pg 1943.

55. K.Elimer, R.Wendt, R.Cebullas “ZnO/ZnO:Al Window and Contact Layer for Thin Film Solar Cells: High Rate Deposition By Simultaneous RF and DC Magnetron Sputtering” 1996 IEEE 25th PVSC Washington D.C.